DETERMINATION OF DIMER DISSOCIATION CONSTANT OF NEURAL CADHERIN BY FLUORESCENCE RESONANCE ENERGY RESONANCE

A Thesis
presented in partial fulfillment requirements
for the degree of Master of Science
in the Department of Chemistry and Biochemistry
The University of Mississippi

by

Xiaoyun Howard

August 2013

ABSTRACT

Cadherins are calcium-dependent adhesion molecules that play a prominent role in the formation of solid tissues. Cell-cell adhesion occurs through the formation of strand-crossover dimers between identical cadherin protomers. Recent studies on neural and epithelial cadherins from our lab showed a dramatic calcium-dependent difference in their kinetics of dimer disassembly, which may have a physiologically relevant role. This motivated our interest to develop methods to study calcium-dependent dimerization of cadherins. The goal of this study is to establish protocols for and energy transfer-based technique for studying dimerization by cadherins. We report Fluorescence (Förster) Resonance Energy Transfer (FRET) experiments between donor and acceptor fluorophore-labeled proteins and the determination of K_d using the change in FRET signal as a function of protein concentration. These studies will provide the basis for a long-term interest of our lab in the geometry of the protomers at the adhesive dimerization interface.

To measure the calcium-dependent dimerization kinetics and equilibrium properties that govern the dynamics of adherent junction, we employed FRET to study adhesive dimer formation by Neural- cadherin (NCAD). We engineered Cysteine mutations that were subsequently covalently labeled with IAEDANS as donor and Alexa Fluoro 488 as acceptor fluorophores at position 87 for solution phase work.

We used two titration methods to determinate K_d for the dimerization process. First,

solutions with low concentration of acceptor were titrated with solutions with high concentration of donor. Second, solutions with high concentration of donor were titrated with solutions with low concentration of acceptor. These two experiments allowed us to span a broad range of protein concentration. The midpoints of transitions indicate NCAD had an association constant (K_d = 25.0 ± 3.0 μM) that was similar to values from the literature (K_d = 25. 8 ± 1.5 μM; K_d = 28. 1 ± 4.0 μM).

DEDICATION

To

Joshua H. Howard and Dylan F. Howard

This thesis is dedicated to my husband, Joshua, and my son, Dylan, who supported me every step of my journey.

LIST OF ABBREVIATIONS AN SYMBOLS

AF488	Alexa Fluoro 488
Apo	Calcium-depleted
A87C	Mutation of alanine at 87 to cysteine in ECAD12
AEDANS-Q87C	AEDANS fluorophore labeled mutant Q87C protein in NCAD 12
AF-87C	Alexa Fluoro 488 labeled mutant protein 87C in NCAD 12
A_t	Total protein concentration of acceptor
CD	Circular Dichroism
C9A	Mutation of cysteine at 9 to alanine in ECAD12
C_t	Total protein concentration of donor and acceptor
D1	Aspartate at position 1 in NCAD 12
D103A	Mutation of aspartate at 103 to alanine in NCAD12
D134A	Mutation of aspartate at 134 to alanine in NCAD12
D136N	Mutation of aspartate at 136 to asparagine in NCAD12
DMF	Dimethylformamide
DMSO	Dimethyl Sulfoxide
DTT	Dithiothreitol
D_t	total protein concentration of donor
EC	Extracellular domains

EC1	Extracellular domain 1 of NCAD12
EC2	Extracellular domain 2 of NCAD12
ECAD12	Epithelial-cadherin domains 1 and 2
E89	Glutamate at position 89 in NCAD 12
EGTA	Ethylene glycol tetraacetic acid
F_A	Fluorescence emission of acceptor
$F_{T(apo)}$	Fluorescence emission of the mixture of donor and acceptor in the absence of calcium
$F_{(A+D)}$	Sum of fluorescence emissions of donor and acceptor
F_C	Limit point of dimerization
F_D	Fluorescence emission of donor
FL	Fluorescence emission
FRET	Fluorescence (Förster) Resonance Energy Transfer
HEPES	N-(2-hydroxyethyl) piperazine-N'-2-ethanesulfonic acid
IAEDANS	1,5-IAEDANS, 5-((((2-Iodoacetyl)amino)ethyl) amino) Naphthalene-1-Sulfonic Acid
IPTG	Isopropyl β-D-1-thiogalactopyranoside
Kan	Kanamycin
K_d	Dissociation constant
LB	Luria broth
NCAD12	Neural-cadherin domains 1 and 2 (residues 1 to 221)
NCAD 12_Q87C	Mutation of aspartate at 87 to cysteine in NCAD12

PBS	Phosphate buffered saline
PCR	Polymerase Chain Reaction
SDS-PAGE	Sodium dodecylsulfate polyacrylamide gel electrophoresis
SEC	Size exclusion chromatography
Satd	High calcium conditions (1 mM Ca^{2+})
TCEP	Tris (2-carboxyethyl) phosphine
T_m	Melting temperature
Tris	Tris (hydroxymethyl) aminomethane
Wild-type	Wild-type NCAD12
WT	Wild type NCAD 12
W2	Tryptophan at position 2 in NCAD 12

ACKNOWLEDGMENTS

I would like to thank all of those people who helped and supported to make this study possible. There is no doubt in my mind that without their continued support and aid I could not have completed this project.

First, I would like to sincerely thank my advisor, Dr. Susan Pedigo. As an advisor, she not only provided guidance and suggestion for my study, but also devoted herself to this research. During the research period, when we encountered many obstacles and challenges, she always gave us thoughtful insights and advice. When experiments did not go well, she spent numerous hours on trouble shooting and trying different methods to solve problems with us. Especially, during the thesis-writing period, I was very frustrated with my writing since English is not my native language. She offered me her kindness and patience throughout the entire process. She also gave me tremendous encouragement and support. We not only met at regular times for comments, suggestions, and corrections. We also talked to each other after school, meeting in her office on weekends and holidays for proofreading and editing my manuscript, correcting spelling and grammar mistakes. We also talked about personal and family matters. When I faced personal difficulties, I deeply appreciated her gentle kindness and strong encouragement to be independent. Dr. Pedigo is not just my advisor, my supervisor; she also is my trusted friend.

Second, I would like to thank my best friend, Dr. Nagamani Vunnam. I'm heartily thankful for her selflessness and kindness that will always be remembered. During the research

time, we started as lab mates, and then were research partners. Eventually we developed a strong and trusting bond and became best friends. We not only enjoyed countless happy times, but we also shared frustration and personal pains. For years, we did experiments together, analyzing the data and practicing presentations. She helped me develop my technical skills and aided me whenever she could. For my thesis, she gave me tremendous help in many ways from contributing ideas, giving feedback and advice to correcting writing mistakes. I will always appreciate all she has done.

Third, I would like to thank my committee members Dr. Michael Mossing, Dr. Nathan Hammer, and Dr. James Cizdiel, for their very helpful insights, comments and suggestions. Especially I would like to thank Dr. Mossing and Dr. Hammer for giving us valuable advice and participating our discussion meetings.

Finally, I wish to thank my family who has supported me throughout the process. I would like to thank my husband, Joshua and my son, Dylan, for their continued support and encouragement of my academic pursuits. They have contributed to many needs while I studied. I would like to thank my mother-in-law, Angela Howard, and my father-in-law, Harrison Howard for always being there for me. I'm very grateful for their unconditional love and generous support. Without their love and support this work would not have been made possible.

Additionally, I would like to acknowledge Yogini Bhavsar who did the preliminary work of cloning NCAD 12_Q87C.

TABLE OF CONTENTS

LIST OF TABLES

LIST OF FIGURES

CHAPTER 1

INTRODUCTION

Cadherins are calcium dependent homophilic cell adhesive molecules, which play an important role in the development of the nervous system during embryogenesis. N-cadherins are critical for synaptogenesis and synapse maintenance. They optimize the synaptic function by constant regulation of synaptic plasticity. Cadherins comprise an extracellular region, a transmembrane region and cytoplasmic regions. The extracellular region has five tandemly repeated ectodomains (EC1-5), with three calcium binding sites situated between each of these domains. The structural and functional characteristics of cadherins are critically dependent on calcium binding. Our research focuses on domains one and two of the extracellular region, a minimal subunit for cadherin function. Recent studies from our lab showed a dramatic calcium-dependent difference in the kinetics of neural (N-) and epithelial (E-) cadherins dimer disassembly, which may have a physiologically relevant role. This motivated our interest to study whether there is a geometrical factor for these kinetically different dimeric states. To investigate these geometrical factors we need to develop and perform a series of bulk and single molecule methods that use Fluorescence (Förster) Resonance Energy Transfer (FRET) phenomenon. These studies will provide a new method to characterize the kinetics of dimerization of epithelial and neural cadherins. In the thesis, I will address the following specific aims.

I. Specific Aims:

1. Establish protocols for labeling protein with fluorophore.
2. Observe FRET between donor and acceptor labeled proteins.
3. Determine K_d using the change in FRET signal as a function of protein concentration.

In the following sections, I will introduce the background and structural information for N-cadherin, and key elements that are required for adhesive dimerization.

II. Background

Classical cadherins are the primary calcium-dependent homophilic cell-cell adhesion molecules in solid tissues. They are found at junctions in a wide array of species from fruit fly to vertebrates. Cadherins are central for the maintenance of tissue structure and integrity. They play a crucial role in morphogenetic and differentiative processes such as embryogenesis (1-3), and cell signaling (4, 5). Cadherins are also involved in several aspects of neural development including synaptogenesis (6), synapse maintenance (7, 8) and the regulation of synaptic plasticity (9). Defects of cadherin-mediated adhesion are associated with tumorigenesis including cancer cell invasion, and metastasis (10, 11). Since E- and N-cadherin mediated cell adhesions exert profound biological effects during development, health and disease, it is important to understand the mechanism of cell adhesion by these molecules.

Classical cadherins share common structural features that comprise three parts: an amino-terminal extracellular (EC-) region, a single-span transmembrane segment, and a conserved cytoplasmic domain containing the carboxyl terminus that interacts with the actin cytoskeleton through catenins (**Figure 1)**.

The EC-region contains five tandemly repeated domains connected by Ca^{2+} binding linker segments. These five domains fold independently into seven- β stranded barrels of IgG type I

consensus fold (12). The EC-domains are numbered from the outermost N-terminal domain as EC1 to EC5, the membrane proximal domain. Each domain contains of approximately 110 amino acids. Three calcium ions bind to amino acid residues in the linker segments and loops in the interfacial region between successive EC-domains. Even though the cytoplasmic domain is not directly involved in dimerization of cadherin, it is important for communication with the actin cytoskeleton and for synapse dynamics (13, 14).

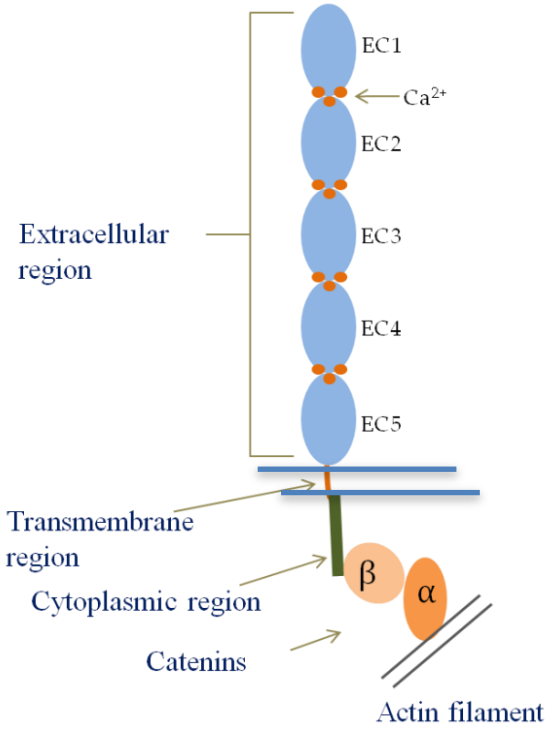

Figure 1. **Illustration of classical cadherin structure.** Cadherin is a single polypeptide with ~650 amino acids. Modular EC domains are represented as blue ovals with three calcium ions (orange) bound at the interface between each modular domain. The cytoplasmic domain (grey bar) is shown with cytoplasmic proteins called catenins which then interact with the actin cytoskeleton.

II.A. Neural-cadherin and epithelial-cadherin

Neural cadherin and epithelial cadherin are the two best studied members in the classical cadherin family. The first two EC-domains of these proteins are remarkably similar in sequence, structure and dimerization interface, yet they have distinct locations at synapses and dramatic

differences in monomer-dimer exchange kinetics. We will discuss these aspects of N-cadherin and E-cadherin: location, sequence, structure, dimerization, and kinetic of dimerization.

II.A.1. Expression of cadherin

In the central nervous system, both E-cadherin and N-cadherin can be expressed in the same neuron yet localized at two different types of synapses: inhibitory synapses (E-cadherin) and excitatory synapses (N-cadherin). Inhibitory synapses are found in dendritic shafts, soma, and proximal axonal regions of neurons (15, 16). At inhibitory synapses, the concentration of calcium is relatively constant. The concentrations of potassium and chloride ions fluctuate in response to signals from neurotransmitters. In contrast, excitatory synapses are found at dendritic spines and the concentration of extracellular calcium fluctuates with each signaling event; pre- and post-synaptic cells uptake calcium and deplete extracellular calcium in synaptic clefts. N-cadherin is considered as a "synaptic tag" for actively stimulated excitatory synapses (17, 18). The segregation of these proteins and differences in extracellular calcium levels at inhibitory and excitatory synapses fuel our interest in the kinetics of dimerization of N- and E-cadherin.

II.A.2. Sequence alignment of E- and N-cadherin

Although the variations in the sequence of ECAD 12 and NCAD 12 are small, they display dramatically different dynamics of the monomer-dimer equilibrium. In order to compare these two proteins the sequence EC1 and EC2 were aligned as shown in **Table 1** using LALIGN (19). This program defines similarity in sequence logically as conserved differences such as Isoleucine/Valine and Serine/Threonine. It also assigns residues that are less conserved as similar, Lysine/Glutamine, for example. Nonetheless given their criteria, E- and N-cadherins have a high level of sequence homology. Comparison of the sequences shows the following: EC1 (1~99) 57% identical and 27% similar, linker 1 (100~106) 86% identical and 14%, similar,

EC2 (107~212) 54% identical and 23% similar, linker 2 (213~ 219) 71% identical and 29% similar. Overall the first two domains of E- and N-cadherin (1~212) are 81% identical and similar.

```
1
DWVIPPISCPENEKGEFPKNLVQIKSNRDKETKVFYSITGQGADKPPVGVFIIERETGWLKVTQPLDREAIAKYILYSHAVSSNGE
:::::::. ::: .: ::.:::.:.:.:::. .. ::.:: :::.::.:.:::.  .: :.::.:::::. ::.. : .:::.::.
DWVIPPINLPENSRGPFPQELVRIRSDRDKNLSLRYSVTGPGADQPPTGIFIINPISGQLSVTKPLDRELIARFHLRAHAVDINGN

AVEDPMEIVITVTDQNDNRPEFTQEVFEGSVAEGAVPGTSVMKVSATDADDDVNTYNAAIAYTIVSQDPELPHKNMFTVNRDTGVI
 ::.:..::::.: :.:::::::: ..:.:::: :: .::: :: :.: ::::  :. :. . : :.:: :  :  ::::.: .:: :
QVENPIDIVINVIDMNDNRPEFLHQVWNGSVPEGSKPGTYVMTVTAIDADDP-NALNGMLRYRILSQAPSTPSPNMFTINNETGDI
                                                    219
SVLTSGLDRESYPTYTLVVQAADLQGE---GLSTTAKAVITVKDINDNAP
 ...:::::.   :::.::.:..:.   :::.:: ::::: :.::: :
ITVAAGLDREKVQQYTLIIQATDMEGNPTYGLSNTATAVITVTDVNDNPP
```

Table 1. **Sequence comparison of ECAD 12 and NCAD 12.** Top line is the ECAD 12 sequence (red) and bottom line is the NCAD 12 sequence (black) from mouse. Black double dots represent identical amino acids residues. Similar residues are shown in black single dots. The seven amino acids in the linker regions are underlined.

II.A.3. Structure of cadherin

ECAD 12 and NCAD 12 also exhibit structural similarity. The comparison of the crystal structures of NCAD 12 and ECAD 12 by Tamura *et al* illustrate the great similarity between the structures of these two proteins (20). Considering the Cα EC1-EC1 alignment and EC2-EC2 alignment, there is < 1Å root mean square difference (rmsd) between the structures. When Cα EC1-EC1 was aligned, rmsd between them was 0.72 Å. While Cα EC2-EC2 was aligned, rmsd between them was 0.84 Å. EC1 is the most studied unit and has been well characterized structurally and functionally because it is the key player in cadherin dimerization.

II.A.4. The dimerization of classical cadherins

The extracelluar domains of classical cadherin interact through direct noncovalent interactions, ionic interaction, hydrophobic interactions, and hydrogen bonding. Dimerization of cadherin occurs through formation of adhesive interactions between extracellular domains of cadherins from neighboring cells. Adhesive interaction occurs at the interfaces of EC1 domains

of two molecules originating from different cell surfaces. Because protomers originate from opposing cell surfaces, this adhesive dimer is also called a *trans* dimer. To form adhesive contacts, the N-terminal βA-strand of one molecule docks the side chain of its tryptophan at the position 2 (W2) into a hydrophobic pocket in EC1 of a neighboring molecule from the opposing cell surface (**Figure 2)**.

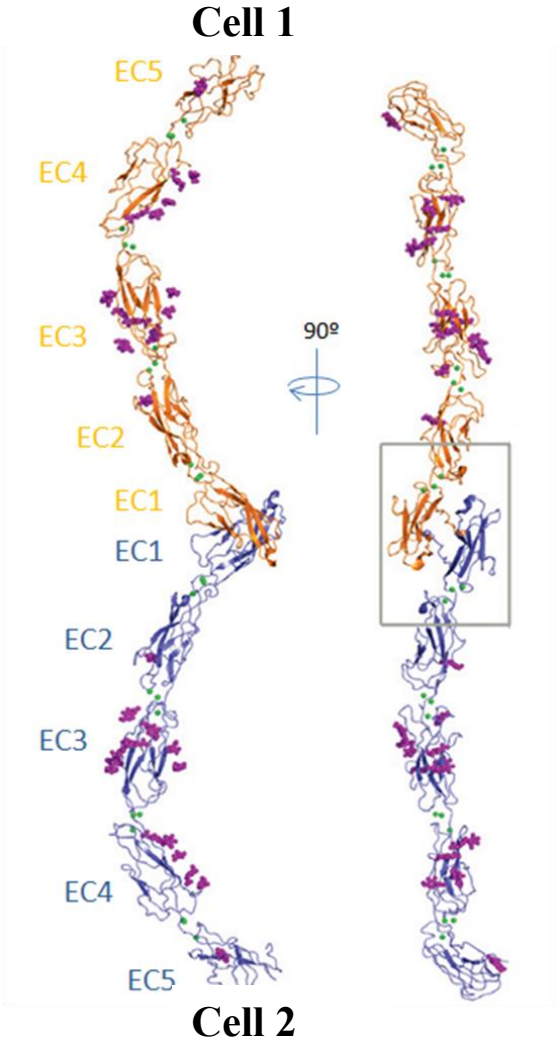

Figure 2. **Adhesive interaction of classical cadherin.** The structure of EC1-EC5 is shown as a ribbon diagram (pdb-ID: 3Q2W (figure taken from Harrison *et al*., (21)). A molecule (blue) from one cell surface interacts with another molecule (orange) from the opposing cell. EC1 domains overlap and exchange N-terminal β-strands. Ca^{2+} ions are shown as green spheres.

The lateral interaction is another type of dimerization (**Figure 3**). It occurs between the

interface of EC1 domain of molecule A and EC2 domain of molecule B in a parallel orientation from the same cell surface. The "front-to-back" contacts are called lateral or *cis* interfaces because the participant protomers come from the same cell. In this case, a hydrophobic surface on the "back" of EC1, away from the site of strand exchange, interacts with a hydrophobic region at the bottom of EC2. Lateral interactions have been observed in N-, E- and C- cadherin molecules in crystal structures (22-24). The data were entirely structural and there was no corroborating biological evidence. Ozawa *et al* used an immunoprecipitation approach to analyze lateral dimer formation by E-cadherin confirmed the existence of lateral dimerization in E-cadherin. Yet, Ozawa reported that the lateral dimerization was not sufficient for adhesive activity (14). Thus, the functional significance of lateral interactions is still debated because the formation of lateral dimers is extremely low affinity under the physiological conditions. Thus, although lateral interactions may occur *in vivo*, they are not relevant to *in vitro* studies.

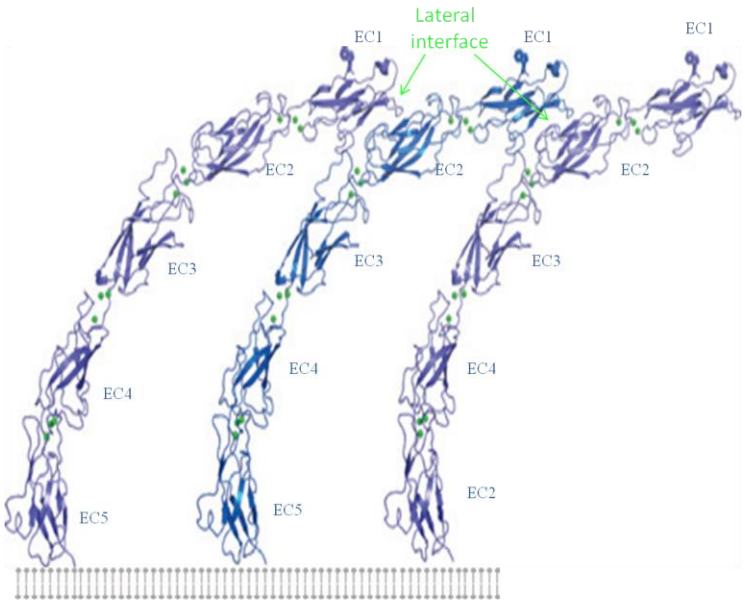

Figure 3. **Illustration of lateral interactions.** A lattice of ectodomains EC1–5 of classical cadherins (figure taken from Harrison *et al*., (21)) shows an array of cadherin molecules oriented from the same cell membrane and connected by EC1-EC2 interactions between neighboring molecules.

II.A.4.1. Details of adhesive dimer formation

II.A.4.1.a. Role of EC1 in adhesive dimer formation

For more than two decades, a number of biochemists have conducted intensive studies on the EC1 domains of N-cadherin and E-cadherin, and utilized various approaches to understand the potential role of EC1 in cadherin mediated cell-cell adhesion. X-ray crystallography (21, 23-29), NMR spectroscopies (27, 30-33), electron microscopic studies (34) all indicated that cadherins form adhesive dimers exclusively through EC1-EC1 interfaces by exchange of N-terminal βA -strands from opposing cells (**Figure 4**).

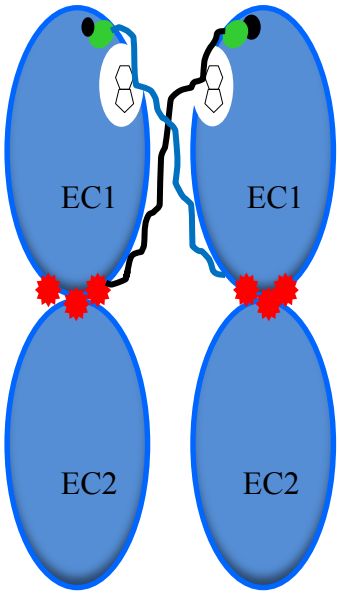

Figure 4. **Illustrations of the strand-crossover interface.** The ionic interaction between the positively changed amino terminus (green) and the side chain of E89 (black) is shown. The aromatic rings from W2 are inserted in a hydrophobic pocket of it partner. Waved lines represent the βA-strand. Red spheres are calcium ions binding at the interface between EC1 and EC2. .

EC1 domains of cadherin have been shown in numerous crystal structures to dimerize through exchange of N-terminal βA-strand between opposing cells which leads to the docking of a Tryptophan 2 (W2) side chain into the hydrophobic pocket of the adhesive partner in the presence of calcium ions (c.f. (23, 27, 28)). For cellular level studies, data from site-directed mutagenesis studies at different locations on the protein (14, 20, 35) and antibody binding

experiments indicating the presence of a disulfide-linked band at the position of strand exchange interface (36) supported the strand-crossover mechanism. From structural and functional studies, biochemists have concluded that in order for the strand-crossover mechanism to occur, four requirements must be satisfied: hydrophobic interactions between W2 and the hydrophobic cleft, presence of calcium ions, salt bridge between N-terminus and E89, and formation of X-dimer.

II.A.4.1.b. Role of W2 in adhesive dimer formation

Tryptophan 2 (W2), an anchor residue, is the second amino acid from the N-terminus in the EC1 domain and is one of the most important players involved in strand-crossover dimerization (**Figure 5**). A number of studies have focused on the role W2 plays in the adhesive interface, especially its contribution to the hydrophobic interaction with amino acids in the hydrophobic binding pocket of the partner protomer. Cell aggregation experiments of NCAD and ECAD were conducted by Tamura *et al* and showed that W2 was a necessary part of the adhesive interaction (20). Tamura *et al* showed that mutation of W2 to alanine (W2A) in cells expressing NCAD and ECAD completely abolished cell-cell adhesion. Immunoprecipitation studies also confirmed the mutation at W2 inhibited dimerization of E-cadherins (14). The Kilshaw research group used peptide-generated antibodies to investigate the effect of W2 on the stability of the EC1 domain (36). Their results show that W2 docks in the hydrophobic pocket of its dimerization partner.

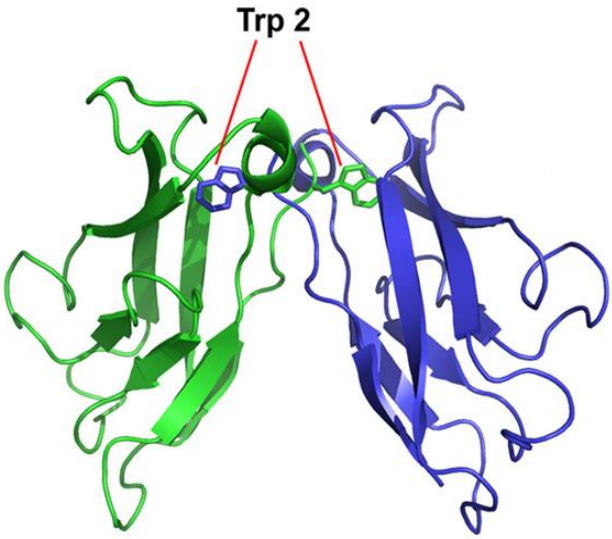

Figure 5. **Ribbon drawing represents the docking of W2 into a partner's hydrophobic pocket.** The W2-containing N-terminal A-strands are docked into hydrophobic cavities reciprocally between neighboring molecules. Green and blue ribbons represent EC1 domain of one or another molecule respectably. The side chains of W2s are shown as aromatic rings (figure taken from Katsamba *et al*., (26)).

Analytical size exclusion chromatographic studies of NCAD also showed that the W2A mutation prevented the formation of dimer (37). Therefore, W2 plays a central role in the stabilization of adhesive interaction by intermolecular docking of the conserved N-terminal "adhesion arm" into the acceptor pocket and stabilizing the adhesive interface of EC1 by interacting with residues inside the hydrophobic cavity of the partner protomer.

II.A.4.1.c. Role of hydrophobic pocket in adhesive dimer formation

Residues of the hydrophobic pocket also play an essential role in the strand-crossover process. W2 and hydrophobic pocket residues from two different molecules are a complementary pair for the adhesive interactions. The key residues (A78, A80 and I92 (NCAD) or M92 (ECAD)) inside of the hydrophobic cavity in N-cadherin must be preserved in order to interact with the side chain of W2 (**Figure 6**). These hydrophobic forces stabilize the interface between EC1 domains. Cell aggregation experiments from Tamura *el al* showed that mutating amino acids Ala-78 or Ala-80 to methionine in the hydrophobic binding pocket prevents cell

aggregation (20). Presumably binding pocket cannot accommodate both the methionine and W2 side chains from the strand dimer partner. Consequently the hydrophobic interactions were disrupted and the dimerization was abolished as well. The crystal structure of Parisini *et al* also shows a hydrogen bond (H-bond) between the backbone carbonyl of D90 and the nitrogen in the indole ring of W2 (see **Figure 6**). This H-bond will also stabilize the docking of W2 into the hydrophobic cleft.

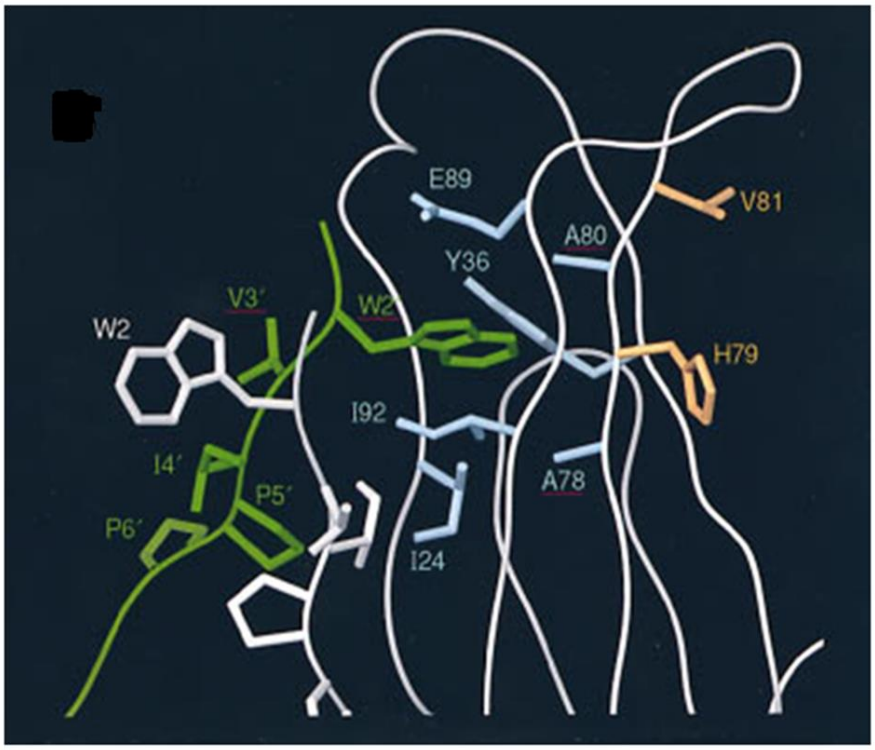

Figure 6. **Details of the hydrophobic pocket of NCAD.** βA strand with W2 of molecule A (green) is docked into the hydrophobic cleft of partner molecule (white). Participant residues are shown in light blue (figure taken from Tamura *et al*., (20)).

II.A.4.1.d. Ionic interaction between the N-terminus and E89

The strand-crossover interaction depends on a salt bridge formed between D1 of one molecule and E89 of the other (**Figure 7**). The positively charged α-amino group (NH_3^+) of Aspartate1 (D1) and the negatively charged side chain, the carboxyl group (COO^-), of E89 form an ionic bond as part of the strand-crossover dimer interface. Mutation of E89 to alanine reduced

the affinity of the adhesive dimer (38). Extensions to the mature N-terminus of one or more amino acids (alanine or glycine) that prevent the formation of the intermolecular salt bridge also abolish adhesive function (39). The ionic interaction between the N-terminus of molecule A and E89 of molecule B optimizes W2 docking and influences as well the dynamic equilibrium of intramolecular and intermolecular docking of W2 (24).

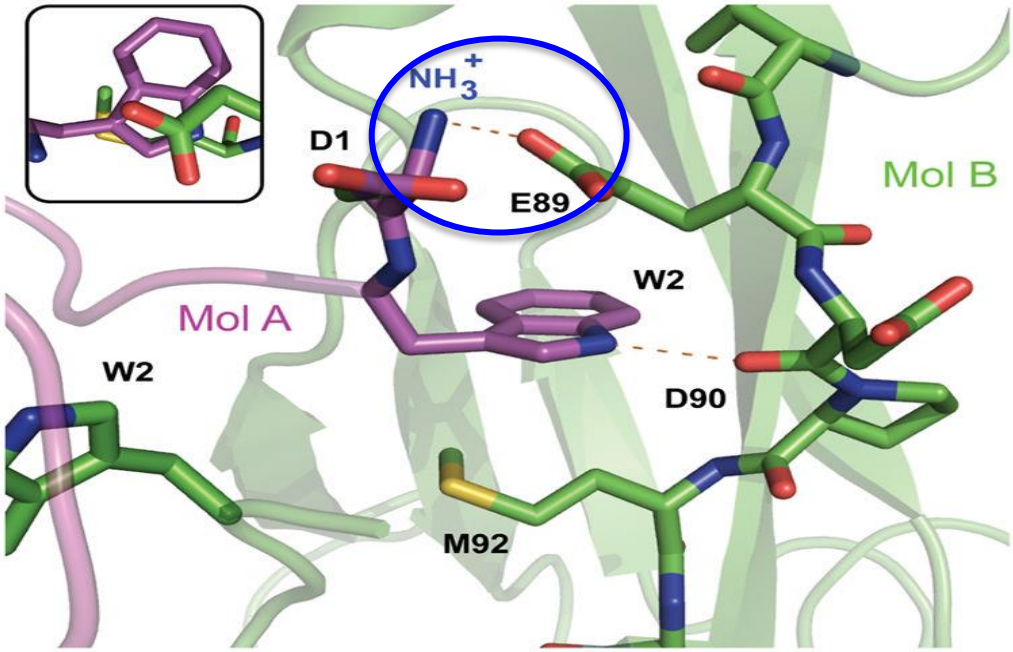

Figure 7. **Details of the ionic and H-bonding interactions at the N-terminus of ECAD.** Interactions between the N-terminus of molecule A (purple) and the hydrophobic pocket of molecule B (green) are shown. Broken lines show the formation the salt bridge between the N-terminal D1-NH_3^+ and E89, also the hydrogen bond between N of W2 and the backbone carbonyl group of D90 (figure taken from Parisini *et al* (24)).

II.A.5. Role of Ca^{2+} in adhesive dimer formation

N-cadherin and E-cadherin are calcium-dependent cell-adhesive molecules. Binding calcium regulates the biological function of cell adhesion in two different aspects: stabilizing and rigidifying the ectodomains, and facilitating the dimer formation.

The presence of calcium rigidifies the linker regions between successive domains into a proper curvature, and at the same time maintains the overall domains in certain conformational flexibility as well. The curvature of ectodomain is critical for adhesive binding because the distal

EC1 domain and proximal EC5 domain need to be oriented ~ 90^{o} relative to each other to meet the geometrical requirements of strand-crossover dimerization (21). This is represented in **Figures 2** and **3**.

The conservation of the calcium-binding residues (D103, D134, and D136) at the interface between the EC1 –EC2 in both NCAD 12 and ECAD 12 have great effects on the calcium-induced dimerization. In our lab, Vunnam *et al* used spectroscopic and chromatographic methods to investigate the relative significance of these three calcium-binding sites at the EC1-EC2 interface in calcium-induced dimerization of N-cadherin. Mutation of D134 and D136 completely abrogate calcium binding. They concluded that calcium-binding site 3 must bind first, and that D134 and D136 are required for binding to site 3. These mutations also prohibited dimer formation except at calcium concentration 10 x higher than that found physiologically. The D103A mutant had decreased calcium-binding affinity, but still bound 3 calcium ions. The loss in cooperativity had a profound effect on dimer formation implying that physical linkage between sites 1 and 2 is required for dimerization. These results demonstrated that all three mutations affected calcium binding and dimerization (40). Courjean *et al* employed non-denaturing electrospray ionization mass spectrometry (ESI-MS) to detect protein- protein association, dissociation, and cooperativity effects of calcium in E-cadherin. They found that these calcium ions bound cooperatively to the interface between E1 and E2. Moreover, the D103A mutation led to a loss of cooperativity, the absence of structural changes, and eventually the loss of adhesive activity of E-cadherin (41). Mutation of the calcium binding amino acid, D134, eliminates the adhesive function of cadherin (42). Prakasam *et al* used quantitative surface force measurements and bead aggregation experiments to assess the impact of the calcium site mutations, D134A and D103A, on the adhesion and binding ability of E-cadherin

cells. Their results revealed that D134A and D103A mutants exhibited much longer bond distances between EC1-EC1 (weaker adhesion) and yielded a few, small aggregates, indicating the elimination of adhesion between the N-terminal domains (43).

II.B. Kinetics of dimerization of cadherin

The two best studied members of the classical cadherin family are N- and E- cadherin, which show 81% sequence identity or similarity (19). Although both N- and E-cadherin form adhesive dimer through a strand-crossover interface (21), they differ significantly in disassembly kinetics *in vitro* (37, 44-46) and *in vivo* (47). Recent studies proposed that a transient, low affinity dimeric structure termed the X-dimer is the reason for its fast disassembly (48, 49). In addition to this structural component, there is also a large difference in the calcium-dependent disassembly kinetics of E- and N-cadherin. At high calcium concentrations the disassembly kinetics of both E- and N-cadherin dimers are fast. However, at low calcium concentration the disassembly kinetics differ significantly; while E-cadherin dissociates rapidly, N-cadherin forms a kinetically-trapped dimer (37). This kinetically-trapped dimer of N-cadherin may form at excitatory synapse (6, 50).

II.B.1. Role of X-dimer interactions in kinetics of dimerization

For decades many biochemists have been focusing their attention on studying the strand-crossover dimerization because of the limitations of technology. In recent years, researchers revealed a very important feature of adherens junctions, the X-dimer, a new type of dimer that is critical for the kinetics of dimerization. New crystal structures of classical cadherin have shown that a non-swapped X-interface is formed at the calcium-binding region between EC1–EC2 where two neighboring molecules contact each other to resemble an “X” shape structure (**Figure 8**) through intermolecular ionic interactions and hydrogen bonds (48, 51). Important noncovalent

interactions are indicated in **Figure 9**.

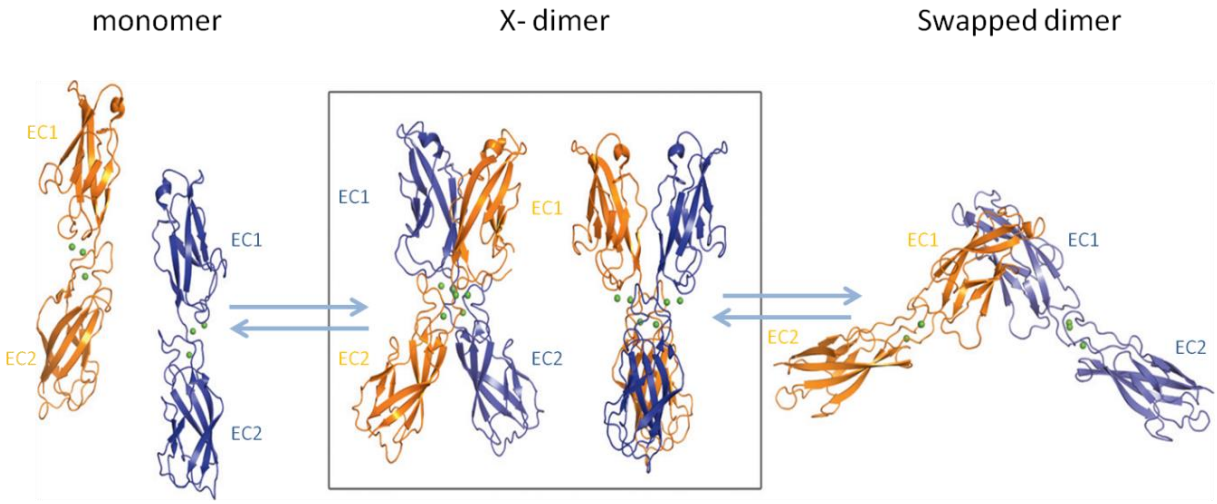

Figure 8. **Formation of mature adhesive dimer is mediated by X-dimer.** Left panel, two monomers from opposing cell surfaces contact each other to initiate dimerization. Center panel, formation of X-dimer acts as an intermediate for assembly and disassembly of the strand-crossover dimer. Right panel, formation of a mature adhesive dimer through reciprocal exchange of βA-strands (figure taken from Harrison *et al*., (21)).

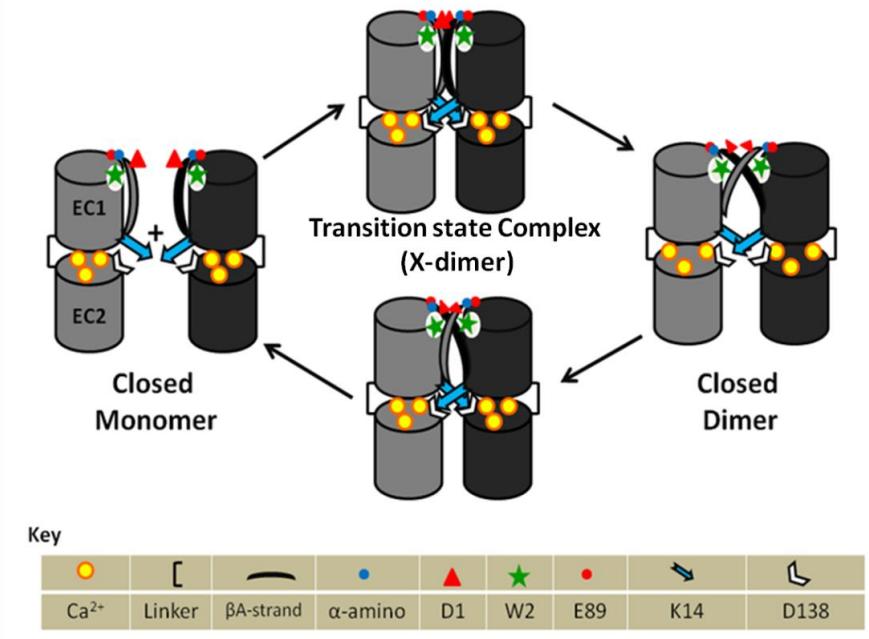

Figure 9. **Model for the strand-crossover structure and X-dimer interface.** On the left panel, for closed monomer, two molecules were unconnected. The βA-strand is docked in its own protomer. On the middle-top panel, two closed monomers contacted to each other to form an X-dimer interface, thereby lowering the activation energy barrier for opening of the βA-strand and forming the strand-crossover dimer shown on the right. In order for the strand crossover dimer to dissociate to monomer, the X-dimer has to reform (middle-bottom panel).

X-dimer (also called the initial encounter complex) is a transition state complex that functions as an intermediate in the equilibrium of assembly and disassembly of the strand-crossover dimer. Sivasankar *et al* proposed the concept of the initial encounter complex based on force probe measurements (52). In the model of the strand-crossover structure, at closed monomer state, two protomers are separated by a certain distance and W2 is buried into its own hydrophobic pocket (**Figure 9**). At the closed dimer state, two protomers are closer to each other to exchange their βA-strand; W2 is hidden inside of the partner's hydrophobic cavity. To form the strand-crossover structure, βA-strand of each protomer has to be opened by breaking non-covalent forces before reforming them in the adhesive dimer partner. In both states, the closed monomer and closed dimer, the W2s are not exposed to solvent (38) and are either docked inside their own or their partner's hydrophobic cleft. Therefore, forming an initial-encounter complex is necessary to keep βA-strand buried either in closed monomer form or in closed dimer form. Meanwhile, forming an X-dimer lowers the activation barrier of assembly and disassembly of dimers.

Harrison *et al* studied the kinetics of disassembly of mutants (K14E and K14S) of E-cadherin. After sedimentation velocity, surface plasmon resonance, and crystallographic studies, they found that mutations reduced the exchange rate of equilibrium between monomer and strand dimer states. From these results they concluded that X-dimers are intermediates of the formation of the strand-crossover dimer (48). Hong *et al* used photoactivation and coimmunoprecipitation experiments to study two X-dimer mutants (K14E and Q101A/N143A) in E-cadherin. These studies suggested that X dimerization is essential in disassembly, but not for assembly (53). Recent studies from our lab showed that the X-enabled mutant of N-cadherin still forms the kinetically-trapped dimer. Thus, the X-interface is not sufficient to confer fast exchange kinetics

for this kinetically-trapped dimeric form in N-cadherin (49).

II.B.2. Calcium dependence of the kinetics of dimer disassembly

As discussed earlier, E-cadherin and N-cadherin both occur at neurological synapses, but not at the same synapse. Because of the nature of inhibitory synapses where E-cadherin occurs, there is a relatively constant concentration of extracellular calcium (~ 1 mM). This is sufficiently high such that we would expect that calcium-binding sites on E-cadherin should be saturated. At excitatory synapses large fluctuations of calcium are likely to occur due to the opening of calcium transporters in both the pre- and postsynaptic cells. Thus, when a nerve impulse travels through an excitatory synapse, there should be large fluctuations in the calcium concentration in the synaptic cleft. Since N-cadherin is indicative of long term potentiation in excitatory synapses, we speculate that there may be properties of N-cadherin that make it particularly sensitive to the large fluctuations in calcium. In support of this concept, we recently performed simple Size Exclusion Chromatographic (SEC) experiments to study the kinetics of dimerization in N- and E-cadherin.

We found that ECAD 12 and NCAD 12 have dramatic differences in the kinetics of dimer disassembly as a function of calcium (37). As witnessed in the data below (**Figure 10**), ECAD 12 dimer disassembles rapidly regardless of the calcium concentration. From the SEC experiments on ECAD 12, data show one peak in both the apo and calcium-saturated states indicating that monomer and dimer are in fast exchange (seconds time scale). In contrast, the disassembly of NCAD 12 was strongly dependent on the concentration of calcium. The data display two distinct peaks in the chromatograms that suggest that monomer and dimer are in slow exchange in the apo state (**Figure 10**, lower right panel). This slow exchange dimeric form,

D^*_{apo}, of NCAD 12 is formed by decalcification of the calcium-saturated dimer. It is kinetically trapped in apo-conditions and unable to disassemble for a long period of time (days to weeks).

The linkage diagram in **Figure 11** illustrates the formation of this trapped species on the SEC column. Thus, the two most prominent members of the cadherin family exhibit strikingly different dynamics of the monomer-dimer equilibrium. We speculate that the D^*_{apo} dimeric form of NCAD 12 may have a physiological role in the "stabilization" of excitatory synapses that is required for long-term potentiation.

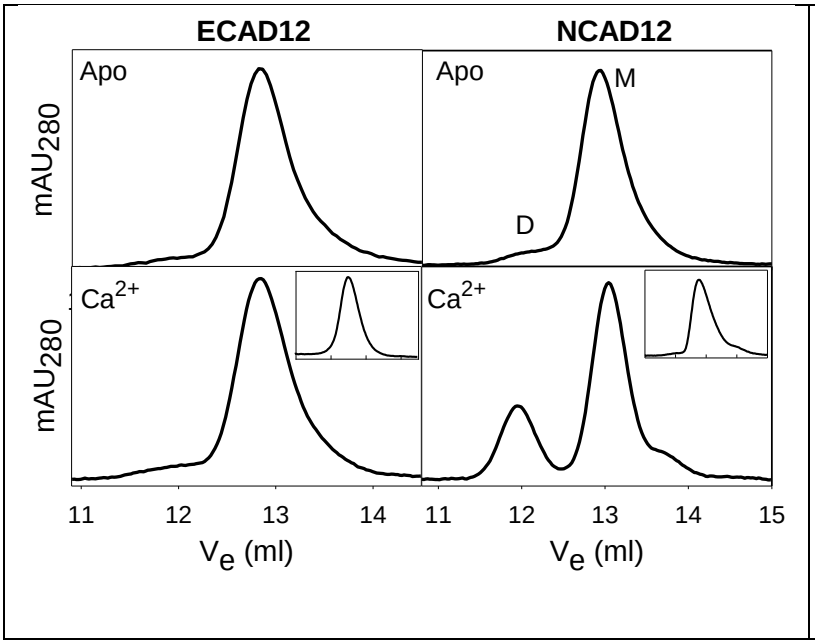

Figure 10. **Analytical SEC to determine the monomer-dimer equilibria as a function of calcium concentration.** ECAD12 (left) and NCAD12 (right) stocks were injected onto the SEC column in apo mobile phase. The proteins stocks were either apo (top) or calcium-bound (1 mM calcium; bottom). The presence of two peaks in the calcium added NCAD12 sample indicates the presence of a slow-exchange dimeric form when the sample is decalcified on the column. The inset in the bottom two panels indicates the appearance of the protein in calcium-added mobile phase. NCAD12 is in fast exchange when calcium is present.

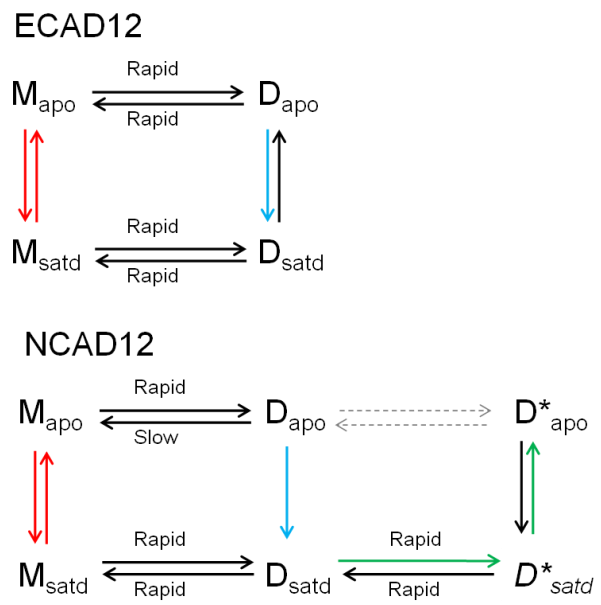

Figure 11. **Exchange dynamics of monomer-dimer equilibria for ECAD12 and NCAD12.** Exchange dynamics of monomer-dimer equilibrium for ECAD12 (top) and NCAD12 (bottom). Solid Arrows are reactions that were observed experimentally. Calcium titrations of monomeric NCAD12 and ECAD12 are represented by solid red arrows. D_{satd} is formed through calcium addition to M_{apo}-D_{apo} stocks. The formation of D_{apo} depends upon the construct. For NCAD12 the green arrows represent the decalcification of D_{satd} to form D^*_{apo}. This was observed through decalcification of calcium saturated stocks on the chromatographic column or by addition of EDTA. The activation energy barrier between D_{apo} and D^*_{apo} is too high to overcome without addition of heat or calcium (dashed arrows).

III. Statement of Purpose

As discussed above the dramatic calcium-dependent difference in the kinetics of dimer disassembly between E- and N-cadherin may have a physiologically relevant role. This striking difference between the calcium-dependent rates of disassembly of strand-crossover dimer motivates our interest in whether there is an orientation difference in the component protomers for these kinetically different dimeric states. We have embarked on a series of solution and single molecule studies to investigate the relationship between kinetics and orientation of the interaction of protomers at the adhesive interface. The primary technology to be used to study kinetics and orientation is Förster Resonance Energy Transfer (FRET). As a prelude to these kinetic and orientation studies, the FRET technique must be established. This thesis chronicles

the development of the FRET studies, particularly solution studies of the equilibrium dissociation constant for NCAD 12.

The following chapters describe components of experimental development and results. Chapter 2 discusses the background information for the fluorescence techniques performed in the work and the determination of the equilibrium dissociation constant. Chapter 3 presents the experimental procedures actually employed. Chapter 4 contains the results and discussion of the experiments that were performed.

CHAPTER 2

PRINCIPLE OF FLUORESCENCE ASSAY

I. Introduction

Fluorescence is a phenomenon of molecules re-emit when absorption of light of given wavelength is followed by emission of light at longer wavelength. Fluorescence-based techniques are widely used in biochemistry at the molecular level and cellular level and are valuable tools for studying structure and function of biological molecules. Fluorescence Resonance Energy Transfer (FRET) is a specialized fluorescence technique that requires a nonradiative transfer of energy between a donor fluorophore and an acceptor fluorophore (54). FRET provides a novel tool in affinity measurements in protein-protein interaction (55). FRET is also often used to study molecular structure and dynamic interactions of biomolecules. First, as reported in this thesis, we will utilize FRET to determine the equilibrium dissociation constant for N-cadherin in the presence of calcium. Later we will use this technique to study calcium-dependent kinetics of disassembly of N-cadherin dimers and the relative orientation between the dimers.

II. Fluorescence Phenomenon

II.A. Stokes Shift

The Stokes' shift is a characteristic of fluorescent molecules. The Jabloński diagram illustrates the energy levels of the absorption and emission of a fluorophore. When a fluorescent

molecule absorbs light, electrons are promoted from the ground electronic state (S_0) to a certain vibrational level of an excited electronic state (S_1), then electrons decay nonradiatively to the lowest vibrational level in the excited electronic state. From there electrons continue to fall back to the ground electronic state, and energy is emitted as a photon (**Figure 12,** left panel). This process results in the difference in wavelength (energy) between the excitation and emission maxima for a particular fluorescent molecule and is called the Stokes' Shift (**Figure 12,** right panel). The Stokes' shift effect was important when selecting a suitable donor-acceptor chromophore pair for the FRET experiment.

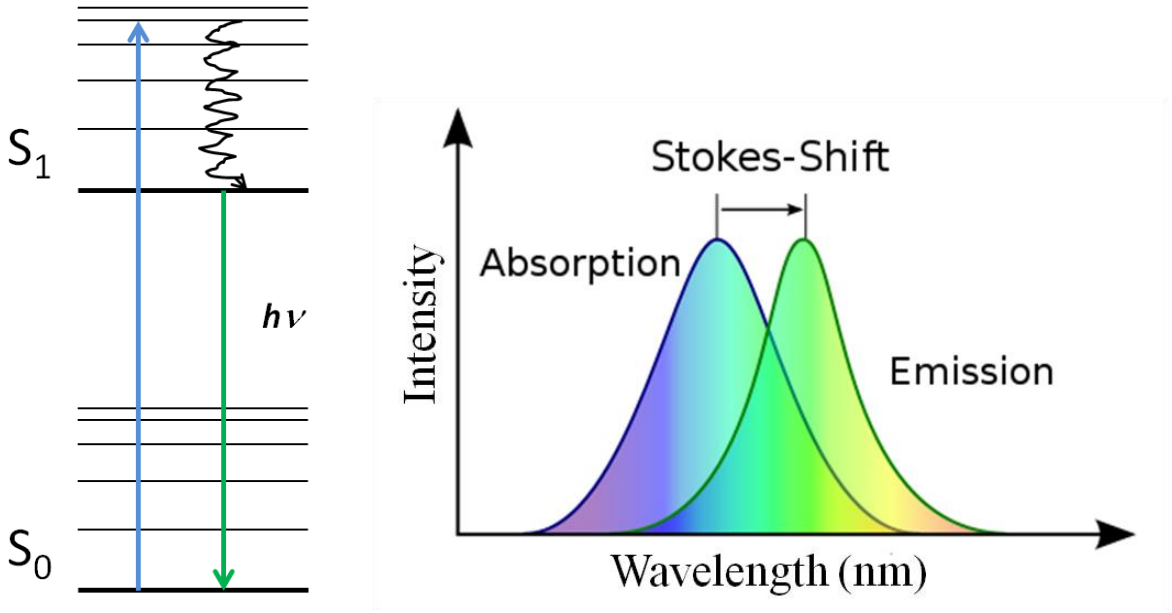

***Figure 12*. Absorption and Emission of energy in fluorescence.** The drawing diagram of energy level of a fluorescent molecule (left panel). Blue up-arrow shows the excitation of fluorophore whose electrons promoted to an exited electronic state S_1 by absorbing light. The black wavy line represents internal conversion to the lowest vibronic state. Green down-arrow represents the emission of the fluorophore whose electrons decay to the ground electronic state S_0 and emits energy as photon. Spectra of Stokes' shift (right panel). The spectra illustrate the process of fluorescence of a fluorophore. Left spectrum shows the absorption spectrum and right spectrum displays the emission. *(https://lp.uni-goettingen.de)*

II.B. Fluorescence Resonance Energy Transfer

II.B.1. Theory of energy transfer between fluorophores

FRET is a process of energy transfer between two fluorophores that have a spectral overlap of emission wavelength of one fluorophore (donor) to excitation wavelength of other fluorophore (acceptor). The energy transfer is nonradiative and happens through long-range dipole– induced-dipole interactions (**Figure 13**; (54)). In general the FRET pair should be chosen to have large spectral separation between donor and acceptor emissions and similar quantum yields and detection efficiencies (56).

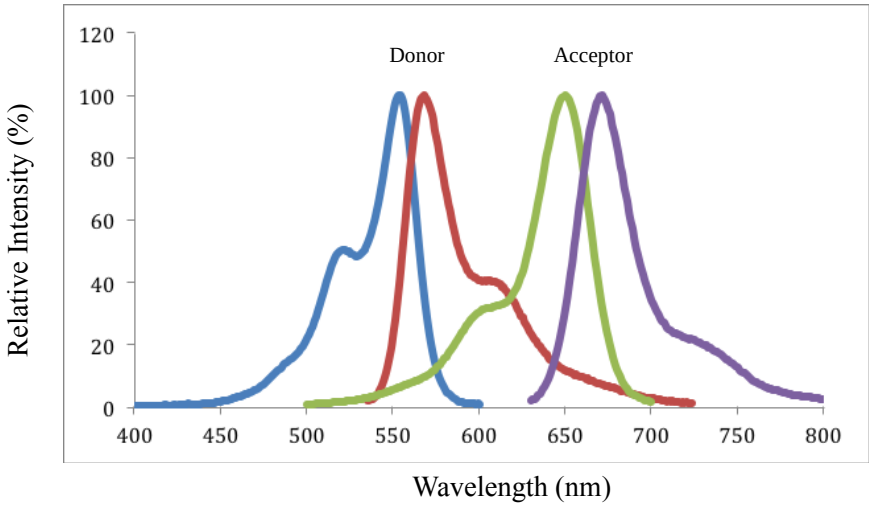

Figure 13. **Spectra of a donor-acceptor pair.** The blue and red lines represent the spectra of the donor. Blue line is excitation spectrum and red is emission spectrum. Green and purple lines represent the spectra of acceptor. Green is excitation spectrum and purple line is emission spectrum. The overlap of donor emission and excitation is between the interval 540 nm to 700 nm.

The process of FRET requires that one fluorescent molecule (donor) in an excited state transfers its absorbed energy to an adjacent fluorescent molecule, the acceptor. This process is illustrated in the Jabloński energy diagram (**Figure 14**). As discussed before, when the donor molecule absorbs photons, electrons become excited and are promoted to a certain vibrational level of an excited state S_1 from the ground electronic state, S_0. The electrons relax rapidly to the lowest vibrational level in the excited state, S_1 within picoseconds due to internal conversion (molecular collisions), and continue to decay to the ground electronic states within nanoseconds. Collapse to the ground state releases energy, which is transferred nonradiatively to an acceptor to

promote its electrons to an excited electronic state. Subsequently, acceptor electrons fall back to the ground electronic state, and energy is emitted. Emission of acceptor is usually visible light since the energy has decreased by the end of this process. The process of energy transfer is referred to as "resonance" because energy transfer occurs without the appearance of a photon and the donor emission and the acceptor excitation have a similar resonance frequency (similar wavelength).

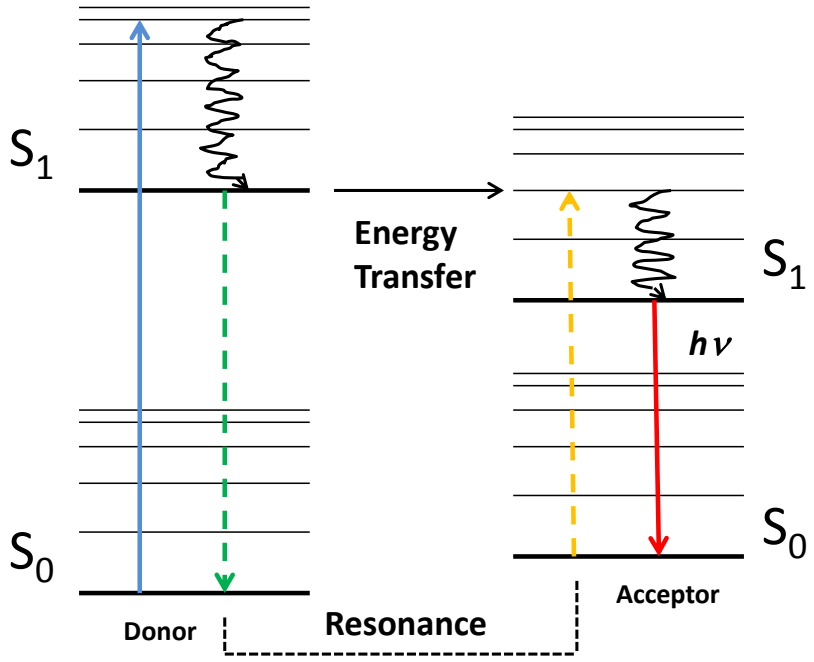

Figure 14. **The schematic diagram of energy transfer in FRET.** The blue up-arrow represents the excitation of a donor as light was absorbed. The waved down-arrow shows vibrational relaxation. Green down-arrow shows the nonradiative collapse of excited elelctrons to ground state. The released energy is transferred from donor to acceptor as "resonance" energy. The orange up-arrow shows the promotion of acceptor electrons to excited state due to the energy transferred from donor. The red down-arrow shows the emission of an acceptor as fluorescence light (figure adapted from *http://ucdavis.edu/Theoretical_Chemistry/Fundamentals/Fluorescence_Resonance_Energy_Transfer)*

Although there are many factors that influence FRET, three primary conditions that must be met in order for FRET to occur: spectral overlap of the emission spectrum of donor and the excitation spectrum of acceptor, distance proximity of the donor and the acceptor, and alignment of dipole moments of the donor-acceptor pair. The probability for FRET increases if the overlap

area of donor fluorescence emission and acceptor fluorescence excitation is large. Overlap promotes efficient transfer of energy from donor to acceptor. The distance between donor fluorophore and the acceptor fluorophore must be close enough to interact with each other within 20–90 Å (10 nanometers) range (Förster distance). Donor and acceptor transition dipole orientations must be approximately parallel. These two factors will be discussed individually.

II.B.2. Efficiency of energy transfer between two fluorophores

The efficiency of energy transfer is the fraction of photons absorbed by the donor that are transferred to the acceptor. The transfer efficiency is usually measured using the relative fluorescence intensity of donor in the absence (F_D) and presence of acceptor ($F_{D\text{-}A}$) by monitoring the FRET signal. FRET efficiency < E > is calculated by the following formula:

$$< E > = 1 - \frac{F_{D-A}}{F_D} \qquad (2.1)$$

The efficiency of energy transfer (< E >) is strongly dependent on the distance between two fluorescent molecules because it is inversely proportional to the sixth- power of distance between them. The fraction is given by:

$$< E > = \frac{1}{1+(R/R_0)^6} \qquad (2.2)$$

where R_0 is the Förster distance of a fluorophore pair. It is the distance at which 50% of the excitation energy of the donor is transferred to the acceptor. The magnitude of the R_0 is dependent on the spectral properties of the donor and the acceptor ranges from 20 to 90 Å, a range which is most useful for studies of biological macromolecules. R is the actual separation distance between the donor and acceptor (D-A distance). The most sensitive distance for R is near R_0, but can range from 0.5 R_0 to 1.5 R_0 (**Figure 14**). The efficiency increases as the donor

and acceptor distance is reduced below R_0. For instance, if R = 0.1 R_0, the efficiency is 0.999999, and the donor emission would not be observable. In contrast, if R is greater than R_0, the efficiency decreases quickly. For example, when R = 2*R_0, the efficiency would be 1.56% and the FRET signal would be very small. Therefore, for better energy transfer efficiency between a donor-acceptor pair, the separation distance should be close to R_0 (54).

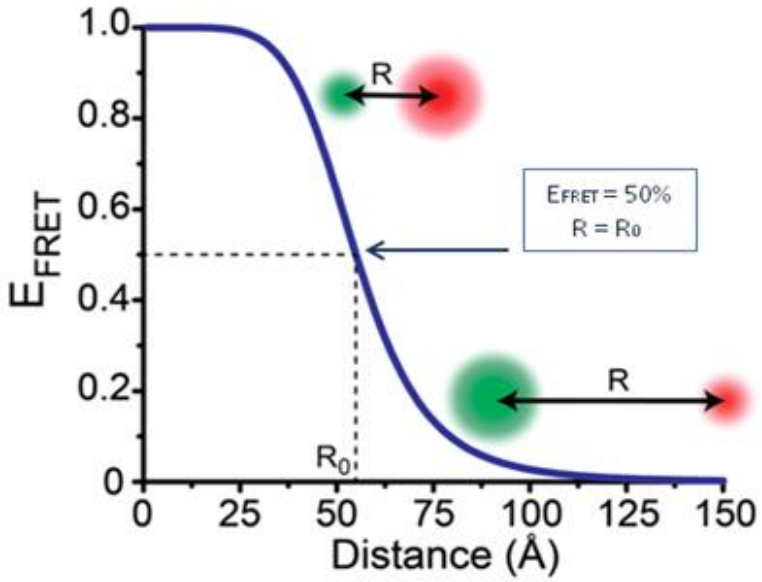

Figure 15. **Diagram of dependence of the energy transfer efficiency on distance.** The graph illustrates FRET efficiency as a function of the separation distance (R) between a donor (green sphere) and an acceptor (red sphere) (Figure from Tinoco *et al*., (57)). When R equals R_0 (55 Å), E_{FRET} is 50%

II.B.3. Impact of Orientation Factor, κ^2, on FRET

FRET depends on the relative orientation of the donor-acceptor, expressed as the orientation factor κ^2, and defined as:

$$\kappa^2 = (\cos\Psi_T - 3\cos\Psi_D \cos\Psi_A)^2 \qquad (2.3)$$

where Ψ_T is the angle between the emission transition dipole of the donor and the absorption transition dipole of the acceptor, Ψ_D and Ψ_A are the angles between the donor and acceptor transition dipoles and the separation vector, $\vec{R}$ (**Figure 16**; (58)).

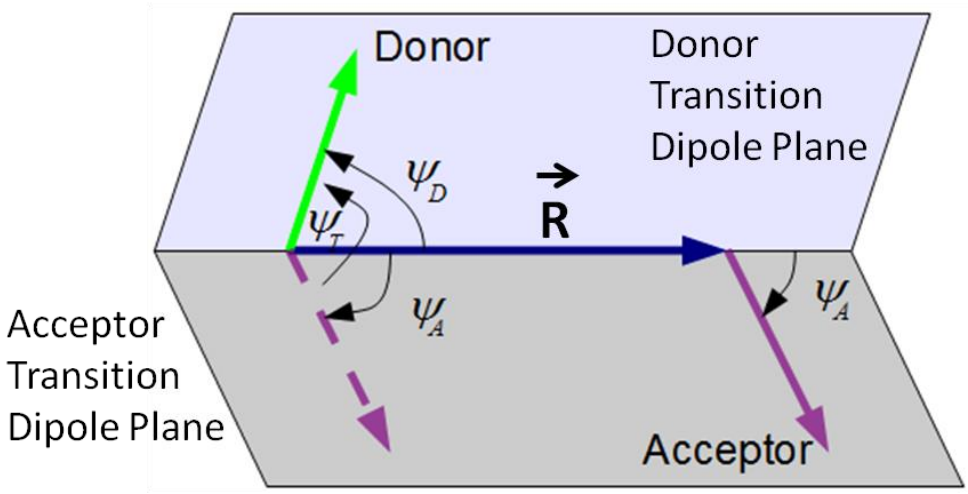

Figure 16. **Vectors and angles relevant to the orientation factor.** The green arrow represents the donor vector in the donor plane; the purple arrow represents the acceptor vector in acceptor plane. The blue arrow represents donor-acceptor separating vector $\vec{R}$ (Figure from Loura *et al*., (58)).

Depending upon the relative orientation of donor and acceptor and due to the six-power to the Förster distance, different donor/acceptor conformations can lead to variation in κ^2. Values for κ^2 range from 0 to 4. K^2 is 0 when transition dipole moments of donor-acceptor pair are perpendicular. A value of 1 corresponds to parallel transition dipoles, while a value of 4 results from dipoles that are collinear (**Figure 17**). However, in most cases of intermolecular interactions, if the molecules undergo fast random orientations of the transition dipole-moments (dynamic averaging), the assumed average value of 2/3 is applied; the orientation of transition dipoles-moment of the donor and the acceptor is approximately parallel (59, 60).

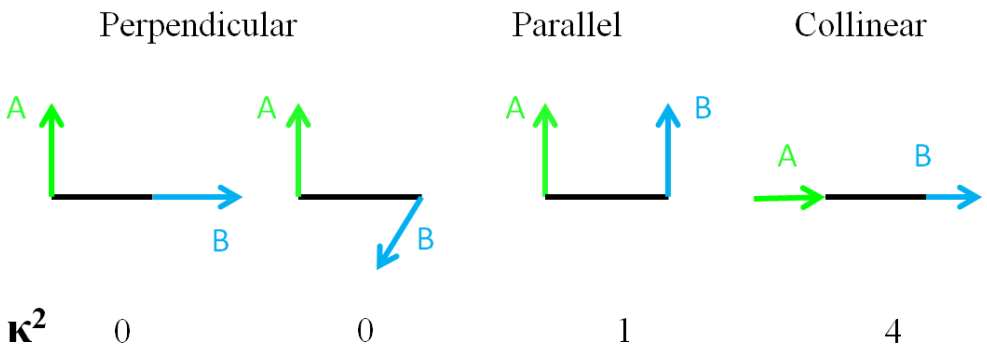

Figure 17. **Transit orientation of dipole moment of the donor-acceptor pair and orientation factor κ^2.** When the dipole moments of donor and acceptor are perpendicular to each other, the value of κ^2 is 0. As the vectors of dipole moment are parallel with each other, κ^2 equals 1. When donor and acceptor are in the same plane, κ^2 is 4 (figure 17 adapted from Eisinger *et al.*, (59)).

FRET energy transfer efficiency has been frequently used to gain structural information about macromolecules by estimating the distances between sites and effects of conformational change because of its intrinsic sensitivity to nano scale changes in D/A separation distance proportional to R^6. Energy transfer is also utilized to investigate biochemical association reactions such as protein-protein interactions, DNA-protein interactions, and protein-ligand interactions. In future studies, we will use experimental determination of efficiency to assess whether there is an orientation difference of protomers at the dimer interface of D_{sat} and D^*_{apo} dimers.

II.B.4. Mathematical derivation to determine the dissociation constant by using FRET signal

Protein–protein interactions play pivotal roles in many physiological processes. The parameter that describes protein–protein interaction affinities is the dissociation constant of dimerization, K_d. Dissociation constants of NCAD and ECAD adhesive dimers have been intensively studied for decades using various methods, including analytical size exclusion chromatography (37), sedimentation velocity (48), surface plasmon resonance (26, 48), and NMR and X-ray crystallographic study (27). The results of these studies are shown in **Table 5** below.

Here we use fluorescence resonance energy transfer (FRET) as a novel method to investigate the dynamics of the formation of strand-crossover dimer and for determining dissociation constants of dimerization of NCAD and ECAD. Formation of heterodimer (A-D) is monitored by FRET signal between fluorescence labeled donor- and acceptor-labeled protein. The fraction of A-D heterodimers is dependent on the relative concentrations of donor and acceptor and K_d. As will be described in detail later, to determine the disassociation constant (K_d) for NCAD, we titrated a small quantity of low concentration acceptor-labeled protein with a high concentration of donor-labeled protein over a wide concentration range. The dimerization equilibrium was monitored by an increase in acceptor signal as a function of donor concentration. Experimental details are described in the next chapter.

We are able to determine equilibrium dissociation constants from the experimental measurements according to the following equations. The following derivation was taken from the Supporting Information accompanying the work by Jia *et al* (61).

$$D \rightleftharpoons M + M; \qquad K_d = M^2 / D \tag{2.4}$$

where K_d is the equilibrium dissociation constant, D is the dimer concentration and M is the monomer concentration. The quadratic relationship in Eq 2.4 above can be rewritten in terms of the total concentration of protein (C_t) and the fraction monomer (X_m) as shown in Eq 2.5.

$$K_d = \frac{(X_m C_t)^2}{C_t(1-X_m)/2} \tag{2.5}$$

Rearranging and solving the quadratic equation for X_m gives Eq 2.6.

$$X_m = \frac{-K_d \pm \sqrt{K_d^2 + 8C_t K_d}}{4C_t} \tag{2.6}$$

The fraction of A in the AD dimer is dependent upon the mole fraction dimer corrected for the fraction of donor in the total protein concentration.

$$\frac{(AD)}{A_t} = \frac{D_t}{C_t} X_d \qquad (2.7)$$

where D_t is the total donor concentration. To relate Eq 2.7 to an actual experimental measurement, we must account for the maximum signal, F_c, according to Eq 2.8.

$$\frac{FRET_A}{F_A} = F_C \frac{AD}{A_t} = F_C \frac{D_t}{C_t} X_d \qquad (2.8)$$

During the energy transfer process, two fluorescence signals can be measured: the signal from A-D dimer (FRET) and the total acceptor signal (F_A). The proportionality constant F_c is the limiting factor when every acceptor is in a heterodimer (A-D).

The combination of Eq 2.6 and 2.8 yields the overall equation below, where F_c and K_d are fitted parameters.

$$\frac{FRET_A}{F_A} = \frac{F_C D_t (4C_t + K_d - \sqrt{K_d^2 + 8C_t K_d}}{4C_t^2} \qquad (2.9)$$

Thus, with the relationship between the total protein concentration, the concentration of donor-labeled protein and the experimental signal, we can determine the equilibrium dissociation constant for dimerization. In the following chapter, all of the experimental details will be presented.

CHAPTER 3

EXPERIMENTAL PROCEDURES

This section outlines the experimental techniques that are systematically practiced in our laboratories for expression and characterization of NCAD 12 and ECAD 12 constructs. These methods that have been standard for our cadherin studies include cloning of the expression plasmid, protein expression and purification, spectral characterization, thermal-induced unfolding studies, and calcium binding studies. Additionally, new methods will be discussed for labeling protein with a fluorescent probe and assembly studies using FRET.

I. Recombinant Plasmids Construction and Cloning

A plasmid containing the gene of mouse neural cadherin of the first two ectodomains (EC1-linker1-EC2-linker 2 sequence) was provided by Prof. Lawrence Shapiro (Columbia University, New York). The target segments of NCAD 12 (residues 1 -221) and ECAD 12 (residues 1 -219) were amplified by Polymerase Chain Reaction (PCR). PCR product of NCAD 12 and ECAD 12 were inserted into pET30b Xa/LIC vector at the LIC site (Novagen) (**Table 2**), and were treated with +dGTP. PCR insert annealed to Xa/LIC vector, and transformed into competent *E. coli* cells. (**Figure 18**, **Table 2**). We chose this plasmid due to a specific feature: a 45 amino acids fusion segment beginning in His_6 at the N-terminus forms a fusion protein with the insert with a convenient proteolytic cleavage site to remove the fusion. His_6 sequence is important for protein purification by metal (Ni^{2+}) chelation chromatography. Arginine is the last

residue of the 45 amino acid fusion and is a cleavage site for trypsin. Cleavage is crucial for producing a clean N-terminus in order to permit formation of strand-crossover dimers.

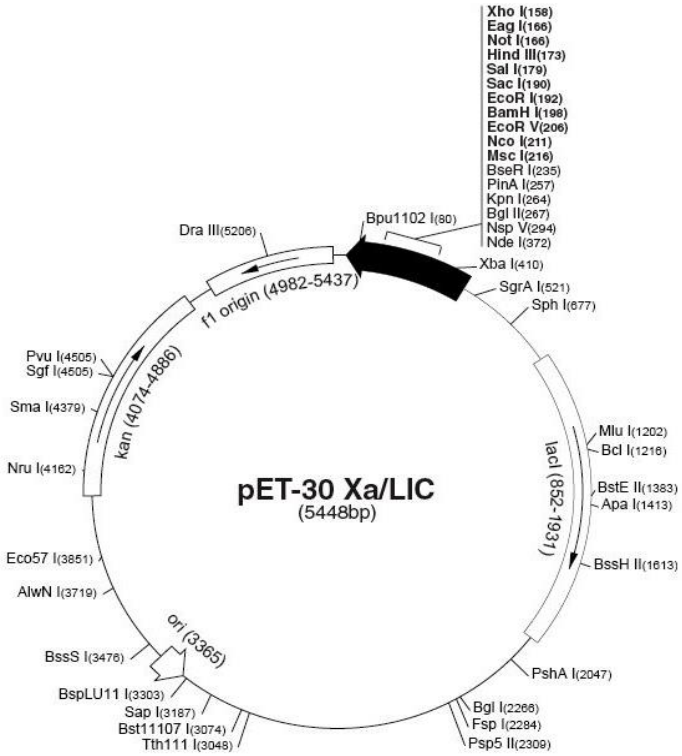

***Figure 18*: pET30 Xa/LIC vector**. Genes for NCAD 12_Q87C and ECAD 12_A87C-C9A were inserted at the LIC site which is between the restriction enzyme sites PinA I and BseR I. The gene for Lac repressor is *lacI*.

Table 2: pET30 Xa/LIC vector with various restriction enzyme sites

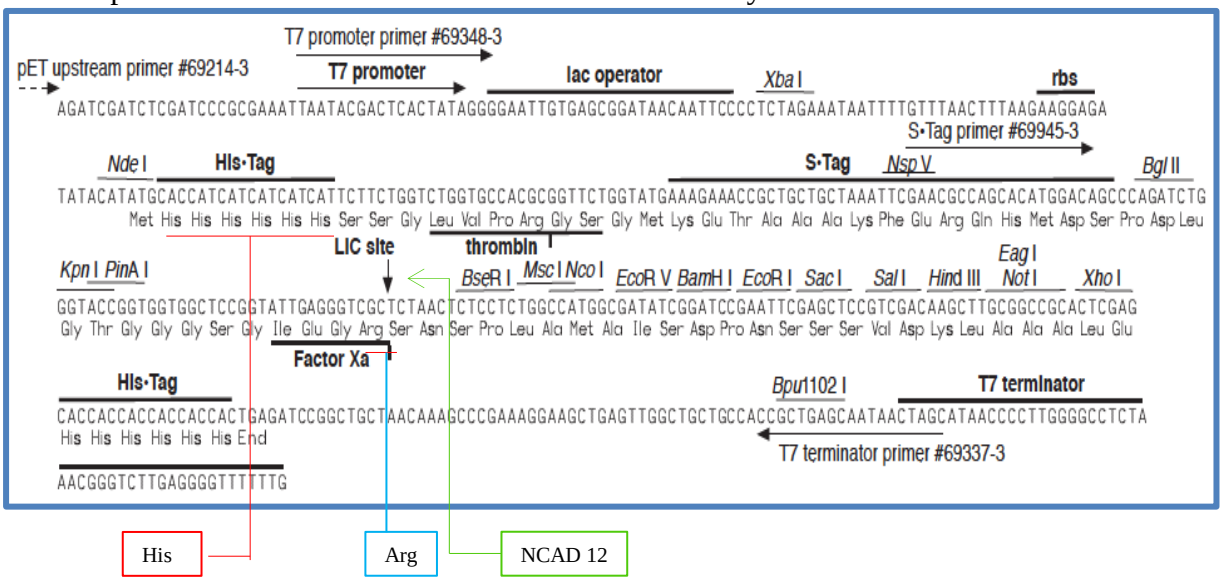

In order to introduce mutations into the genes, point mutations were performed using Quick Change II site-directed Mutagenesis Kit (Stratagene) according to three steps: 1. Designing two desired mutagenic primers (sense and antisense), 2. Synthesizing multiple copies mutant plasmid by using PCR, and 3. Transforming the mutant plasmids into the expression cells (*E. coli*).

To design primers, primers must contain the desired mutation with approximately 45 bases in length and position the mutation in the middle of the primers. The primers should have a minimum of 40% GC content and be terminated in one or more C or G bases and have a melting temperature above 78 °C. Plasmids were amplified by using PCR. The thermal cycles were selected based on plasmid size. During this process, the primers annealed to the thermally denatured DNA template and subsequently synthesized new DNA from the 3' end of the primers. This process replicates the entire plasmid. The parental methylated plasmid was digested by the restriction enzyme DpnI. The formation of plasmids in the PCR experiment was assayed by using agarose gel electrophoresis. *Escherichia coli* BL21 (DE3) expression cells were transformed with pET30b Xa/LIC vectors encoding NCAD 12_Q87C and ECAD 12_A87C_C9A for protein expression.

To determine the K_ds of ECAD and NCAD by FRET studies, we introduced several mutations to these constructs. For the FRET study, having a properly positioned cysteine residue is essential for labeling the protein with fluorophore. NCAD 12 and ECAD12 were mutated to introduce a cysteine residue at position 87. Position 87 was selected for labeling with a dye due to its location near the insertion site for the A-strand in the folded protein and proximity to the hydrophobic pocket where the strand-crossover interaction occurs. Moreover, at this position, cysteine was ~ 76% exposed (62) so that it allowed us to derivatize proteins conveniently with

minimum perturbation of the protein structure. For the NCAD 12_Q87C construct, a single mutation was carried out, Q87 to cysteine. For ECAD 12_ A87C_C9A construct, double mutations were introduced, A87 to cysteine, as well as C9 to alanine. To eliminate the possibility of labeling the protein with fluorophore at an undesirable site C9 was mutated to alanine.

Primers used in these experiments were as follows: Point Mutation of NCAD 12 to Q87C, **Sense:** 5'GCA CAT GCA GTG GAC ATC AAT GGC AAT TGC GTG GAG AAC3', **Antisense:** 5'GTT CTC CAC GCA ATT GCC ATT GAT CTC CAC TGC ATG TGC3'; Point Mutations of ECAD 12 to C9A, **Sense:** 5'CCC TCC CAT CAG CGC GCC CGA AAA TGA AAA G3', **Antisense:** 5' C TTT TCA TTT TCG GGC GCG CTG ATG GGA GGG3'; Mutation of ECAD 12 C9A to A87C, **Sense:** 5'CT CCA GAA GGC TCT AAC TCT CCT CTG GGC3', **Antisense:** 5'GGC CAG AGG AGA GTT AGA GCC TTC TGG AG3'. Clones were sequenced to confirm the presence of the mutation.

II. Protein expression and Purification

Transformed cells were grown separately on LB agar plates containing 30 μg/mL kanamycin at 37 °C for 16 hours. A single colony was picked and used to inoculate 50 mL of Luria-Betrani broth with 30 μg/mL kanamycin (LB-Kan) for an overnight growth. Five mL of the overnight cell culture was added into a 700 mL LB-Kan broth at 37 °C with shaking until the cell growth reached an OD_{600} around 0.5 AU. Cells were induced by adding 0.4 mM IPTG. After 2 hours of induction, cells were harvested by centrifugation at 3000 rpm for 15 minutes at 4 °C. Cell pellets were suspended in ~10 mL of 20 mM HEPES, 100 mM KCl, pH 7.4 buffer and frozen at -20 °C. Protein was found in the inclusion bodies. To purify the inclusion bodies, cells were lysed by sonification. Insoluble protein was separated from other cell components by

washing the pellets with different concentration of Triton-X (10% and 1%) followed by centrifugation. Washed pellets were dissolved in His-tag binding buffer, 6 M urea, 20 mM Tris-HCl, 500 mM NaCl, and 5 mM imidazole, pH 7.5 for an overnight period. His-tag chromatography was performed for purification of the protein. A Ni-affinity column (Amersham) was employed by utilizing affinity reaction between Ni^{2+} ions of the column resin and His_6-tag at the N-terminus of the protein, then the proteins were washed with 20 mM Tris-HCl, 500 mM NaCl, and 40 mM imidazole, pH 7.9 buffer to remove nonspecifically-bound protein. The proteins of interest were eluted in fractions by applying the elution buffer, 10 mM Tris-HCl, 0.250 M NaCl, 500 mM imidazole, pH 7.9.

Fractions with high protein concentration were combined into one solution which was dialyzed in digestion buffer containing 140 mM NaCl, 20 mM Tris, 10 mM $CaCl_2$, 5% glycerol, 1 mM DTT, pH 7.4 with stirring at 4 °C overnight. The immobilized trypsin enzyme (Pierce) was applied to cleave off the N-terminal fusion with the mixing ratio 2:1 (500 μL protein / 250 μL immobilized trypsin enzyme) for 1.5 hours with constant shaking at 25 °C. The digested protein was dialyzed in SEC buffer, 140 mM NaCl, 10 mM HEPES, pH 7.4 to reduce calcium concentration to 1 μM. The purity of proteins was assessed by SDS-PAGE gel. Masses of purified protein were confirmed by mass spectrometry. Hereafter in this thesis, only the results from studies of N-cadherin will be discussed.

III. Spectral Characterization of recombinant and wild type proteins

III.A. Spectral Characterization by using UV spectrophotometer

Cary 50 Bio UV spectrophotometer was used to assess the effect of the mutation on the basic characteristics of purified proteins and to determinate their concentrations. Protein concentrations were determined by monitoring UV spectra in a 0.4 cm path length quartz cuvette

with the wavelength range from 350 nm to 200 nm. Molar extinction coefficients of NCAD 12 and ECAD 12 were determined by using the Edelhoch method (63) to be 17,400 ± 500 $M^{-1}cm^{-1}$ for NCAD 12 at 280 nm (37).

III.B. Spectral Characterization by using Circular Dichroism Spectrometer

Circular dichroism (CD) measurements were performed by using an AVIV 202SF CD spectrometer to assess the effect of mutations on NCAD 12_Q87C structure and stability. CD wavelength scans were conducted from 200 nm to 300 nm using a 0.5 mm path length quartz cuvette with a 5 second averaging time at 25 °C. CD spectral changes were monitored in the absence and presence of calcium (1 mM). In order to ensure protein samples were calcium free, 5 mM EGTA was added to the apo samples.

For thermal denaturation studies, all experiments were conducted using a 1 cm path length quartz cuvette with a temperature probe passing through the screw cap. The temperature range was set from 15 °C to 90 °C. The temperature ramp rate was 1 °C/min with a 30 seconds to 1 min equilibration time with a 5 second acquisition time at a fixed wavelength between 225 to 235 nm with stirring. To observe the impact of calcium binding, experiments were performed at two calcium concentrations, the apo state (5 mM EDTA) and calcium saturated states (1 mM). All protein samples were prepared in 140 mM NaCl, 10 mM HPEES, pH 7.4 buffer. The thermal unfolding transitions were fit to the Gibbs-Helmholtz equation with linear native and denatured baselines with adjustable slopes and intercepts that had been established in our lab by Prasad *et al* (64).

$$\Delta G = \Delta H_m \left(1 - \frac{T}{T_m}\right) + \Delta C_p (T - T_m - T \ln \frac{T}{T_m}) \qquad (3.1)$$

The value of ΔC_p was resolved from the Kirchoff plot of the resolved values of ΔH_m and T_m by fitting the Gibbs-Helmholtz equation.

IV. Calcium Binding Studies

Calcium titrations experiments were monitored by CD spectrometry. At room temperature, 2.5 μM protein samples in 140 mM NaCl, 10 mM HEPES, pH 7.4 buffer in a 1.0 cm cuvette were titrated by adding three different volumes, 2μL, 5 μL, and 10 μL calcium chlorides stocks at various calcium concentrations, 1 mM, 10 mM, 100 mM, and 0.7 M. For each titration, a spectrum was documented from 220 to 300 nm. The experiments were performed in triplicate. The spectra were corrected for offset differences at 300 nm. CD data were evaluated individually at wavelengths between 227 and 235 nm.

The calcium titration data were fitted to Eq 3.2,

$$\bar{Y} = \frac{K_a * X}{1 + K_a * X} \qquad (3.2)$$

where $\bar{Y}$ is the fractional saturation of sites and K_a is the calcium association constant. To accommodate the experimental data without prior normalization, the function used for fitting the data is shown in Eq 3.3, where the apo and saturated baselines are linear functions and the span is the difference between them.

$$F(X) = \text{baseline}_{apo} + \bar{Y} \times \text{span} \qquad (3.3)$$

V. Assembly Studies

Analytical size exclusion chromatography (SEC) was used to estimate the levels of fraction of monomer and dimer in a protein sample with a certain protein concentration with and without calcium added. SEC was conducted by using an ÄKTA Purifier HPLC system with a Superose-12 10/300 GL column (Amersham). UV absorption of the protein was detected at 280 nm. A 50 μL volume of 50 μM protein sample was injected with the mobile phase containing 140 mM NaCl, 10 mM HEPES, pH 7.4, and the flow rate of 0.5 mL/min. To monitor the effect

of calcium on dimerization, 1 mM calcium was added to the protein sample. The ratio of monomer and dimer was estimated by measuring the height of the peaks detected at 280 nm.

VI. Fluorescence spectroscopic studies

VI.A. Fluorescent Probes: IAEDANS and Alexa Fluoro 488

IAEDANS and Alexa Fluoro 488 are fluorescent dyes and widely used as markers in fluorescence spectroscopic studies. Chemically they are thiol-reactive dyes that are often used to label proteins for the detection of conformational changes, assembly of multi-subunit complexes and ligand-binding processes *(http://www.invitrogen.com).*

VI.A1. IAEDANS

IAEDANS is the abbreviation for the chemical 1,5-IAEDANS, 5-((((2-Iodoacetyl)amino)ethyl) amino) Naphthalene-1-Sulfonic Acid. It is called IAEDANS before derivatization and AEDANS after derivatization (**Figure 19 A**). The extinction coefficient of the dye is 5,700 $cm^{-1}M^{-1}$. It is soluble in dimethylformaide (DMF). AEDANS-probed protein has a maximum excitation wavelength of 336 nm and a maximum emission wavelength of 490 nm. It can be used as a FRET partner for fluorophores that have an excitation wavelength of 490 nm.

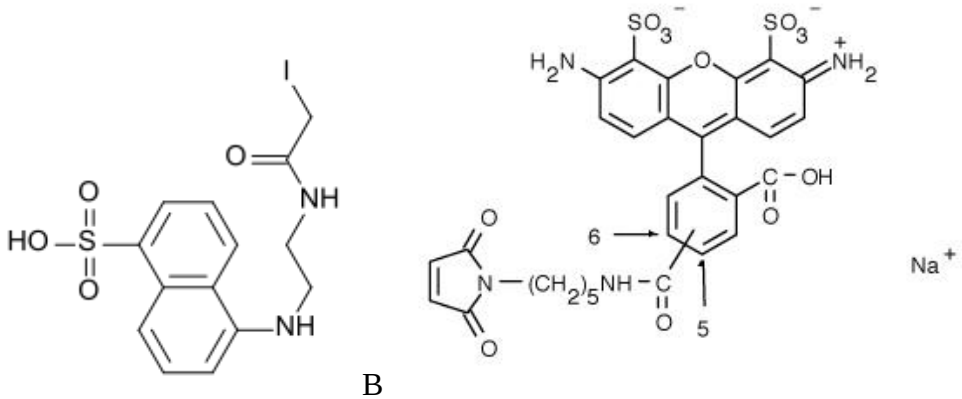

Figure 19. **Structures of AEDANS (A) and Alexa Fluor 488 (B)**. AEDANS and AF-488 have maleimide groups which interact with cysteine through thiol reactions *(http://www.invitrogen.com).*

VI.A2. Alexa Fluor 488 C_5-maleimide

Alexa Fluor 488 C_5-maleimide (AF488) is Xanthylium, 3,6-diamino-9-[2-carboxy-4(or 5)-[[[5-(2,5-dihydro-2,5-dioxo-1H-pyrrol-1-yl)pentyl]amino]carbonyl]phenyl]-4,5-disulfo-, inner salt (http://www.invitrogen.com) (**Figure 19B**). It has a maleimide group, a thiol-reactive probe that targets cysteine residues of proteins as conjugating partners. The extinction coefficient is 71,000 $cm^{-1}M^{-1}$. It is soluble in dimethyl sulfoxide (DMSO). It has excitation and emission maxima of approximately 494 nm and 519 nm, respectively. AEDANS-AF488 was chosen as the donor-acceptor pair because there is excellent overlap between the emission spectrum of the donor and the absorption spectrum of the acceptor (**Figure 20**).

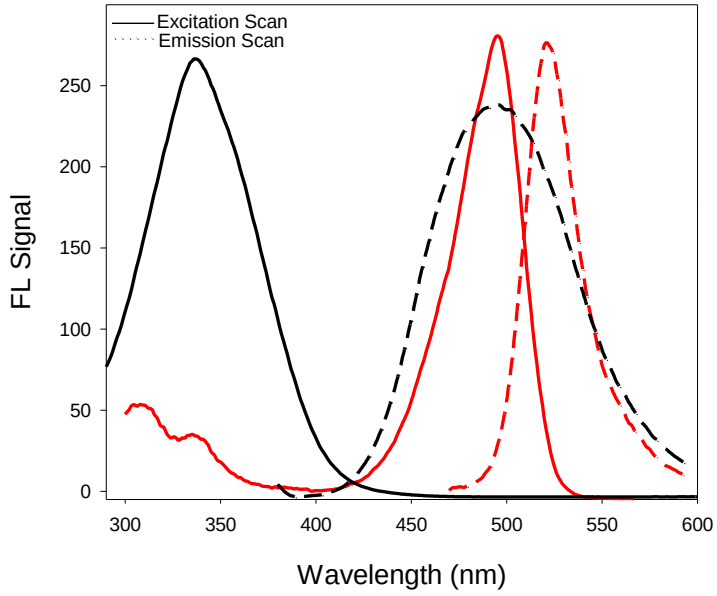

Figure 20. **Absorption and emission spectra of AEDANS and AF 488**. The graph showed that AEDANS (black) had maximum excitation at 336 nm (solid line) and maximum emission at 490 nm, and AF 488 (red) was excited and emitted at 494 nm and 525 nm respectively.

VI.B. Derivatizing NCAD 12_Q87C with AEDANS

VI.B.1. Preparation of protein and fluorophore samples for derivatization

In the first derivatization experiment about 1 mL NCAD 12_Q87C was dialyzed against 1X Phosphate buffered saline (PBS) buffer (pH 7.4) with 1 mM dithiothreitol (DTT) overnight.

Subsequently, the protein was dialyzed against 1 L SEC buffer (pH 7.4) with 1 mM TCEP with stirring for 2 hours. To remove dissolved oxygen NCAD 12_Q87C was dialyzed once more in 1 L SEC buffer (pH 7.4) with 1 mM TCEP while N_2 gas was bubbling in the SEC buffer solution with stirring for 1 hour. TCEP and DTT are reducing regents. Since NCAD 12_Q87C protein contains cysteine, TCEP and DTT are used to reduce disulfide bond. Dialyzed protein stock was immediately transferred into an aluminum foil covered vial (1.5 mL) and tightly capped with a removable rubber septum topped cap, and then the cap was sealed by parafilm. Next, DMF (200 μL) was placed in a clear vial (1.5 mL) with a rubber septum and degassed with slow flowing N_2 gas for 10 minutes. IAEDANS (1.1 mg) was weighed and placed in a microfuge tube in the dark. A 50 μL volume of degassed DMF was withdrawn with a 100 μL volume syringe, and then added to the 1.1 mg IAEDANS.

VI.B.2. Set up for degassing the protein and dye samples

Since the cysteine residues on the protein are sensitive to oxygen, we had to contrive a chamber for purging the protein and dye solvent. Into the top of a small brown glass vial, we inserted a rubber septum. A syringe needle was inserted through the septum. The exposed end of the syringe needle was sealed to one end of flexible plastic tube with parafilm. The other end of the tube was connected to the gas port of a nitrogen tank and sealed with parafilm as well.

VI.B.3. Derivatizing the protein sample with IAEDANS

About 50 μL of IAEDANS- DMF dye solution was withdrawn by syringe and injected into the degassed protein sample vial. Protein was incubated with the dye solution in the dark for 2 hours with stirring at room temperature. AEDANS-tagged protein was dialyzed in 2 L SEC buffer for 2 ~ 3 times in a brown bottle until an UV spectrum displayed low concentration of the

free dye in the SEC buffer solution. Labeled protein was preserved in a microfuge tube tightly wrapped with aluminum foil at - 20°C.

VI.C. Determining the efficiency of AEDANS-labeled NCAD 12_Q87C

Cary 50 Bio UV spectrophotometer was used to determine the degree of the labeling. The spectrum of AEDANS-NCAD 12_Q87C (AEDANS-Q87C) stock was measured in a 0.4 cm path length quartz cuvette with the wavelength range from 600 nm to 200 nm. Protein concentrations were determined using the ε_{280} and the absorbance at 280 nm. The concentration AEDANS was measured from the spectrum at the maximum absorption at 336 nm. The concentration of protein in the sample was calculated by the following equations:

$$Protein\ Concentration = \frac{A_{280} - 23\%\ of\ absorbance\ at\ 336}{17{,}400\ (M^{-1}cm^{-1}) * l\ (cm)} \quad (3.4)$$

where 17,400 $cm^{-1}M^{-1}$ is the molar extinction coefficient of NCAD 12_Q87C. The ε_{280} dye is only 23% of ε_{336}. The concentration of AEDANS was calculated from:

$$\frac{Moles\ dye}{Mole\ protein} = \frac{A_{336}}{5{,}700\ (M^{-1}cm^{-1}) * l\ (cm) * [Protein](M)} \quad (3.5)$$

where 5,700 $cm^{-1}M^{-1}$ is the approximate molar extinction coefficient of the AEDANS at 336 nm.

$$\%\ Derivatized\ protein = \frac{Concentration\ of\ AEDANS\ (\mu M)}{concentration\ of\ AEDANS{-}Q87C\ (\mu M)} \quad (3.6)$$

VI.D. Labeling NCAD 12_Q87C with AF488

Protein stock was dialyzed and degassed as discussed above. The AF488 dye solution was prepared in an identical way except the solvent was DMSO. The concentration of AF488 protein was determined in an identical way except ε_{494} (AF488) was 71,000 $M^{-1}cm^{-1}$ and the ε_{280} (AF488) was only 11% that at 494 nm. The concentration AF488 was obtained by the maximum absorption spectrum at 494 nm according to the following equations:

$$Protein\ Concentration = \frac{A_{280} - A_{494} * 0.11}{17{,}400\ (M^{-1}cm^{-1}) * l\ (cm)} \quad (3.7)$$

$$\frac{Moles\ dye}{Mole\ protein} = \frac{A_{494}}{71{,}000\ (M^{-1}cm^{-1}) * l\ (cm) * Protein\ Concentrtion\ (M)} \quad (3.8)$$

where 71,000 $cm^{-1}M^{-1}$ is the approximate molar extinction coefficient of the AF488 dye at 494 nm. The determination of the labeling efficiency of AF-labeled NCAD 12_Q87C (AF-Q87C) is the same equation as Eq 3.8 except using the AF dye concentration and the AF-Q87C concentration.

VII. Determination of occurrence of FRET

The basic concept behind FRET experiments is that donor labeled monomers can be excited at a wavelength chosen to excite only donor fluorophore. If there is no acceptor present, then the donor would just simply fluoresce at a characteristic wavelength. In the presence of acceptor, the energy from the excited donor will transfer to the acceptor, and the acceptor will then fluoresce at a wavelength that is significantly red shifted from the donor emission maximum. So, we can simply monitor the decrease in the donor emission signal and the increase in the acceptor emission signal (FRET signal) as an indicator of dimer formation.

However there are two sources of possible error that can affect the interpretation of the FRET signal. First, the excitation of donor might directly excite acceptor leading to the emission of acceptor that is not due to energy transfer from the donor. Second, it is possible that the emission of donor can overlap with the emission of acceptor leading to bleed through which can cause significant overestimation of the FRET signal. Due to these concerns, we performed three spectral measurements for each addition of protein in the titration. These spectral measurements provided a total fluorescence signal (F_T), the background signal caused by direct excitation of acceptor (F_A), and background signal caused by bleed through of donor signal into the acceptor

channel (F_D).

The following experiment was done to determine the contribution of direct excitation of the acceptor to the total fluorescence signal. We used solutions of acceptor derivatized protein alone to determine the amount of the acceptor fluorescence signal when exciting at the donor wavelength. Two excitation wavelengths were used: 370 nm (excitation wavelength for energy transfer) and 450 nm (excitation wavelength for the acceptor). The ratio of the fluorescence observed for excitation at 370 nm and at 450 nm permits estimate of the acceptor fluorescence signal from direct excitation at 370 nm. Thus, the difference of signal intensity of emissions obtained from the excitation wavelength 370 nm and 450 nm was used to calculate the correction factor which has the relationship as shown below:

$$Correction\ Factor = \frac{F_{A(450/525)}}{F_{A(370/525)}} \qquad (3.9)$$

To determine F_A in Eq 2.9 we directly excited the acceptor using an excitation wavelength of 450 nm. Then we used the correction factor in Eq 3.9 above to estimate the amount of acceptor signal that was contributing to the apparent FRET signal from direct excitation of acceptor (Ex: 370 nm).

Next, we had to account for the donor emission that overlaps with the FRET channel and artificially inflates the apparent FRET signal. Because donor signal cannot be measured independently once acceptor has been added, we have to use an alternative technique to estimate the contribution of the donor (F_D) to the total fluorescence signal (F_T). In the interval 450 ~ 470 nm, donor signal dominate the emission spectrum. Moreover, in this region donor fluorescence intensities of emission in the absence and presence of acceptor are identical. Therefore, the contribution of the donor (F_D) to the total fluorescence (F_T) was obtained from the emission signal at 457 nm since the fluorescence intensity of donor at 457 nm is equal to the fluorescence

intensity of donor at 525 nm. Thus, the contribution of the donor to the total fluorescence (F_T) at 525 nm can be estimated from the emission monitored at 457 nm. This value for F_D and the value for F_A above must both be subtracted from F_T in order to know the amount of F_T due to energy transfer (FRET signal).

VIII. Quantitatively analysis of FRET Studies by titration of the donor and acceptor

VIII.A. Set up parameters for FRET studies

The donor, AEDANS-Q87C and the acceptor, AF-Q87C were prepared in SEC buffer with 1 mM Ca^{2+} at pH 7.4. All fluorescence studies were conducted using a PerkinElmer Life Sciences LS 55 fluorescence spectrophotometer with a quartz cuvette. The fluorescence emission spectrum of each mixture was measured with the following set up parameters:

Table 3. **Parameters of the fluorescence emissions of donor only and mixtures of donor and acceptor**

Start (nm)	380	End (nm)	600	Excitation (nm)	370
Ex. Slit (nm)	9.0	Em. Slit (nm)	4.0	Scan Speed (nm/min)	100

Table 4. **Parameters for the fluorescence emission spectra of acceptor**

Start (nm)	470	End (nm)	600	Excitation (nm)	450
Ex. Slit (nm)	9.0	Em. Slit (nm)	4.0	Scan Speed (nm/min)	100

VIII.B. FRET assay: Titrations of AF-Q87C with AEDANS-Q87C

Guided by simulation experiments, in order to obtain a broad range of total protein concentration to find the end point of dimerization, two sets of titration experiment were performed: a forward titration and reverse titration. For the forward titration, the concentrated

AEDANS-Q87C was added into the dilute AF-Q87C. Specifically, 120 μL 5μM of AF-Q87C was placed in the cuvette. It was then titrated with 40 μM of AEDANS-Q87C by adding 12 μL aliquots incrementally for a total of 10 additions. For the reverse titration, the AF-Q87C was added into a relatively concentrated stock of AEDANS-Q87C. Here, 120 μL 75 μM AEDANS-Q87C was placed in the cuvette and then titrated with 5 μM AF-Q87C by adding 12 μL for a total of 10 additions. For each titration, the mixture was gently pipetted up and down several times to mix after each addition. After 5 minutes of incubation, the emission spectrum of each mixture was measured according to parameters shown in **Table 3** and **4**.

CHAPTER 4

RESULTS AND DISCUSSION

The goal of this project is to develop a FRET-based method for determining the K_d for dimerization of N-cadherin. We engineered a single mutation at position 87 in NCAD 12 to form NCAD 12_Q87C. The mutant protein was characterized to determine the effect of the mutation on the structure, stability and function of the molecule. The single cysteine in the protein was then derivatized with either IAEDANS as the donor fluorophore or Alexa Fluor 488 as the acceptor fluorophore. Labeling efficiency was determined. An extensive set of fluorescence studies was performed to assess the occurrence of energy transfer between FRET partners. Finally, titrations of FRET partners were performed to determine the disassociation constant. Here we report the results of these method development experiments and resultant K_d values.

I. Characterization of the mutant protein

Even though Q87 is an exposed hydrophilic residue, we were concerned that its mutation to cysteine may impact the structure, stability and dimerization properties of the protein. To ensure the integrity of the mutant protein, we performed an extensive series of studies that are chronicled in this section. These studies include spectral, stability, and assembly studies.

I. A. Spectral Characterization

I.A.1. UV-spectral Characterization of mutant and wild type protein

UV- spectroscopy was used to assess the concentration of a purified protein and folded state of the protein by characterizing the spectrum. The tryptophan and tyrosine residues in folded proteins have signature features in a wavelength range from 270 to 295 nm. NCAD 12_Q87C showed these characteristic peaks at the maximum absorption 280 nm with a low shoulder at 290 nm which is typical for a folded protein containing tryptophan and tyrosine (**Figure 4.1**, (40)). This spectrum indicates that the mutant NCAD 12-Q87C is folded into a compact 3° structure. Comparison of the spectra in **Figure 21A** and **21B** indicate that the mutation did not significantly impact the structure of the protein.

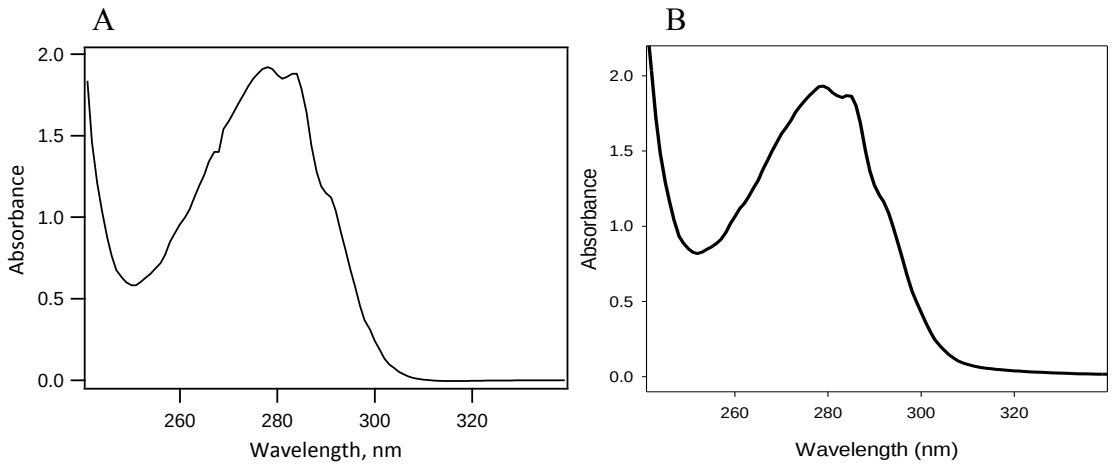

***Figure 21*. UV spectra of the wild type (A) and NCAD 12_Q87C (B)**. The proteins exhibited the absorption bands that are typical for tryptophan and tyrosine containing proteins (~100 µM).

I.A.2. Characterization of mutant and wild type protein using Fluorescence spectroscopy

NCAD 12 contains 2 tryptophan residues (W2 and W113) and 5 tyrosine residues. Tryptophan residues have a significant fluorescence emission at ~ 330 nm that is sensitive to environment. We can assess the general environment of the tryptophan residues by measuring the fluorescence emission spectrum. **Figure 22** shows a comparison of the fluorescence data of

wild type and NCAD 12_Q87C in the apo-state (open symbols). These two emission spectra have the same λ_{max} at 330 nm indicating that mutation did not affect the exposure of the tryptophans.

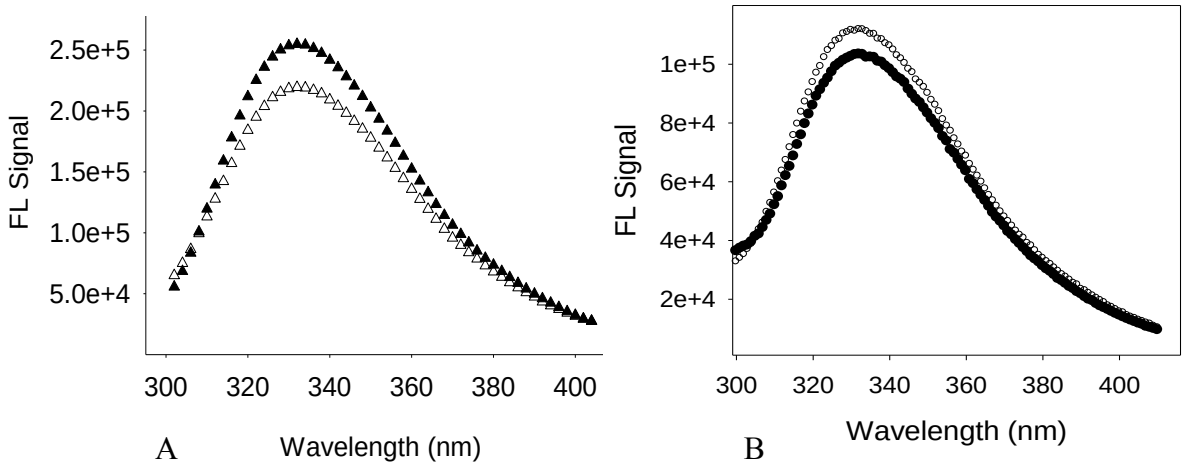

Figure 22. **Fluorescence spectra of the wild type and NCAD 12_Q87C as a function of calcium.** Comparison of the fluorescence emission spectra of wild-type (A) and NCAD 12_Q87C (B) constructs in apo state (open) and calcium saturated state (filled). The concentration of the wild type protein was 5μM, and the path length of the cuvette was 1 cm. The concentration of NCAD 12_Q87C protein was 5μM, and the path length of the cuvette was 1 cm.

To investigate the calcium-dependent changes in the tryptophan environment, we repeated the experiments with 1 mM calcium added. **Figure 22** shows a comparison of the fluorescence data of wild type and NCAD 12_Q87C in the saturated-state (closed symbols). These two emission spectra have the same λ_{max} at 330 nm, and their fluorescence intensities changed indicating that they both bind calcium and undergo a conformational change. There have been a number of studies that report calcium-induced conformational change phenomena in cadherin (38, 65, 66). However, the intensities of the calcium-added spectra moved in opposite directions. From studies in our lab of single tryptophan mutants of NCAD 12, we found that the signal of W2 decreases and that of W113 increases when calcium is added. Thus, it appears that the mutation causes a small conformational change that alters the balance of the contribution to

the fluorescence spectrum from each tryptophan. It is important to note that in the folded structure, Q87 is close to W2 and its docking site, the hydrophobic cleft. The mutation may cause a subtle change in the environment of W2.

I.A.3. Spectral characterization of protein by using CD spectrophotometer

Wavelength scans were performed to investigate whether the mutation would affect the CD spectrum (**Figure 23)**. The CD spectral data showed a wavelength minimum at approximately 218 nm as typical β-sheet protein structure (67) and a local maximum around 235 nm, which reflects 3-10 helix content and tryptophan environment (68). CD spectra of wild type and the mutant both showed a wavelength minimum around 218 nm and a local maximum at 235 nm in both the apo and calcium-saturated states. The spectral signal intensities changed upon the binding of calcium for these two proteins that indicate that they bind calcium and undergo a structural change.

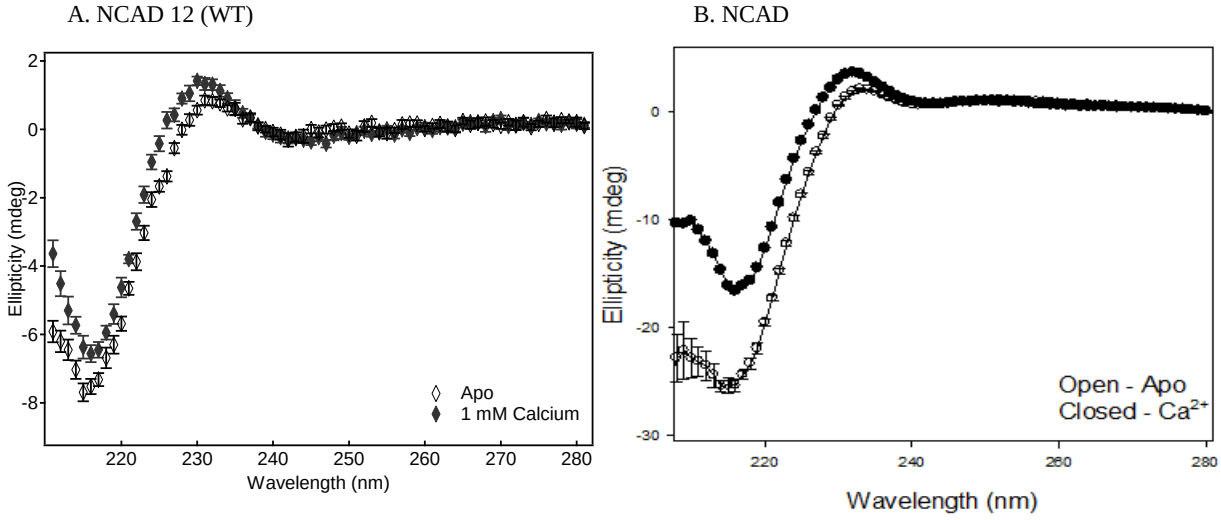

Figure 23. **CD spectra of the wild type and NCAD 12_Q87C proteins**. Proteins were in the apo-state and the calcium-saturated state (1 mM Calcium added). Protein concentration and path lengths were different. Wild type data (A) is from Vunnam *et al* (40). The concentration of the wild type was 60 μM, the path length of the cuvette was 0.5 mm. The concentration of the NCAD 12_Q87C (B) was 296 μM, and the path length of the cuvette was 0.5 mm.

I.B. Calcium Titrations of mutant and wild type protein

Calcium titrations were performed of the mutant protein while monitoring the CD signal. Example data is shown in **Figure 24**. The resolved value for the free energy change of calcium binding was -6.1± 0.5 kcal/mol. This corresponds to a binding constant of 30,000 M^{-1} (K_d = 30 μM). This value is identical to similar titrations of wild type protein reported elsewhere (37).

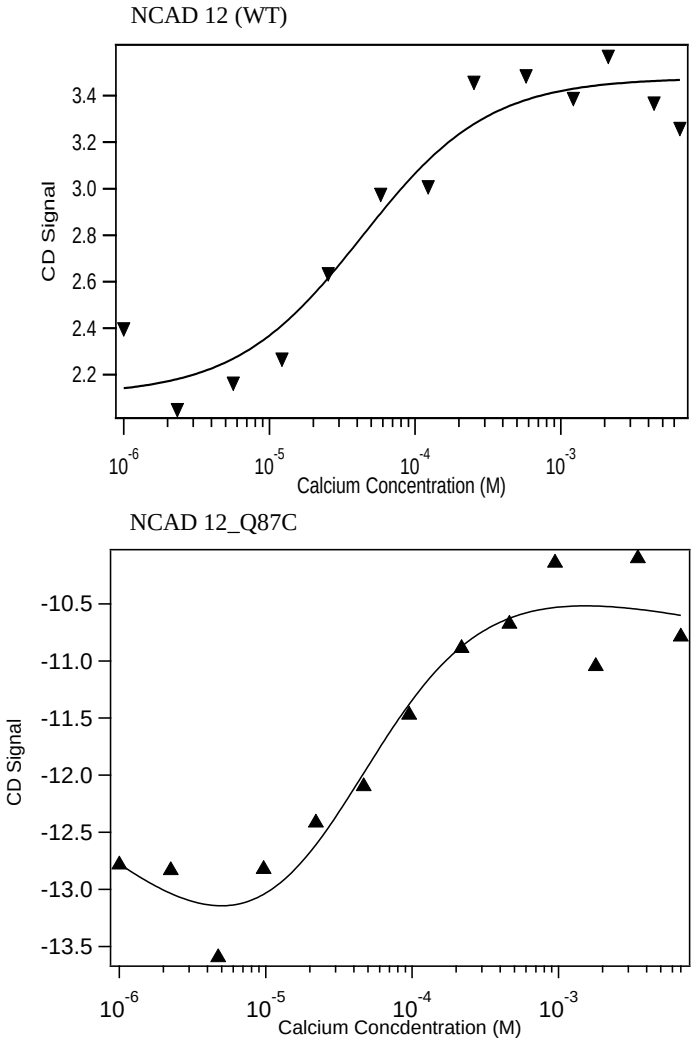

Figure 24. **Calcium titration of the wild type and NCAD 12_Q87C**. A solution of 2.5 μM protein was titrated with calcium. CD signal at 226 nm was monitored and plotted against the total calcium concentration. The concentration of the wild type was 2.5 μM, and the path length of the cuvette was 1 cm (top). The concentration of NCAD 12_Q87C was 5 μM, and the path length of the cuvette was 1 cm (bottom).

I.C. Thermal Unfolding Studies

Thermal-induced unfolding experiments were performed to assess the effect of Q87C mutation on the stability of the protein in the absence and presence of calcium. CD signals at 230 nm were plotted against probe temperature as shown in **Figure 25**. All data were fitted to the two-state model based on the Gibbs-Helmholtz equation (Eq 3.1) to resolve enthalpy change (ΔH_m) and melting temperature (T_m). Resolved parameters are summarized in **Table 5**. The wild type is shown in the left panel (40); the mutant is shown in the right panel. The top panels show the raw CD signal at 230 nm which contain two transitions; the bottom panels show the normalized data of the first transition. Inspection of the plots and resolved parameters indicates that wild type protein and mutant are indistinguishable in the apo state. These results indicate that the Q87C mutation did not affect the stability of apo-protein. Upon addition of 1 mM calcium, melting temperatures and enthalpy changes of both wild type and the mutant increased significantly, which indicates that both proteins are more stable in the calcium-saturated state.

The resolved values for enthalpy changes were similar, while a small difference in T_m was observed. Overall, the thermal-induced unfolding data show that the mutant has similar stability as the wild type. This implies the mutant has minimum effects on protein structure and stability.

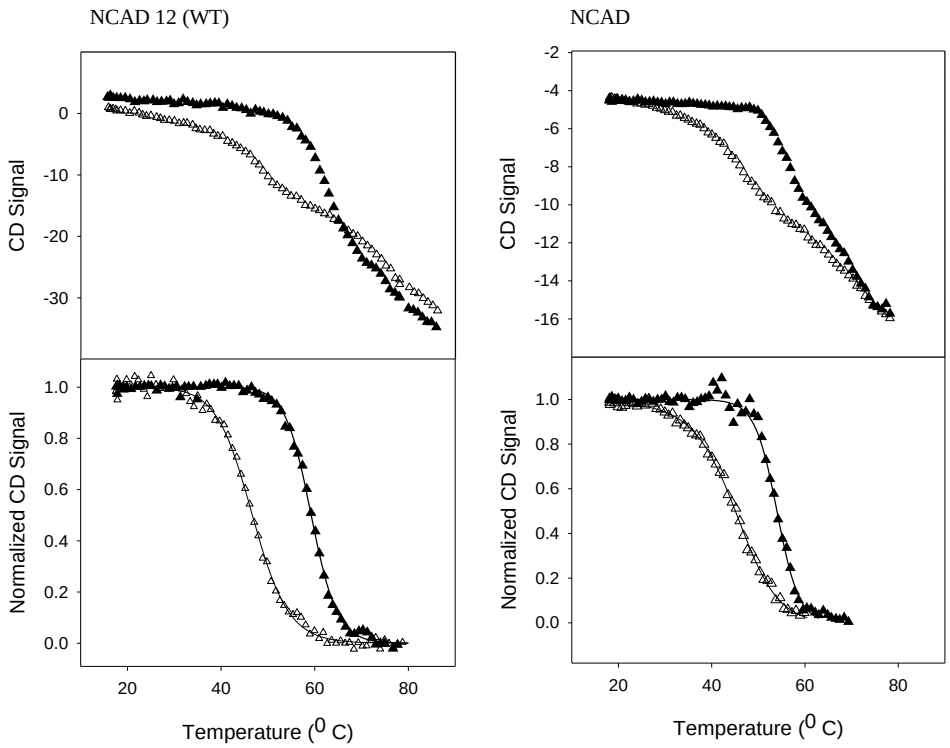

Figure 25. **The thermal-induced unfolding studies of the wild type and NCAD 12_Q87C mutant**. CD signal data of thermal unfolding of WT (left panel) (Figure 4, (40)) and NCAD 12_Q87C (right panel) were obtained in the absence and presence of calcium at 5 μM protein concentration. The top panels exhibited raw data. Bottom panels showed the normalized data of first transition fitted to the Gibbs-Helmholtz equation and corrected for the fitted baselines.

Table 5. **Summary of parameters resolved from thermal unfolding experiments for the wild type and mutant N-cadherin in the absence and presence of calcium**

Protein	Buffer	ΔH_m [a] (kcal/mol)	T_m ($^\circ$ C)
NCAD12_Wild-type	Apo	68 ± 8	45 ± 2
	Ca^{2+}	79 ± 5	59 ± 3
NCAD12_Q87C	Apo	64 ± 9	44 ± 2
	Ca^{2+}	83 ± 10	55 ± 1

[a] The value of ΔC_p was fixed to 1 kcal/mol K.

I. D. Assembly Studies

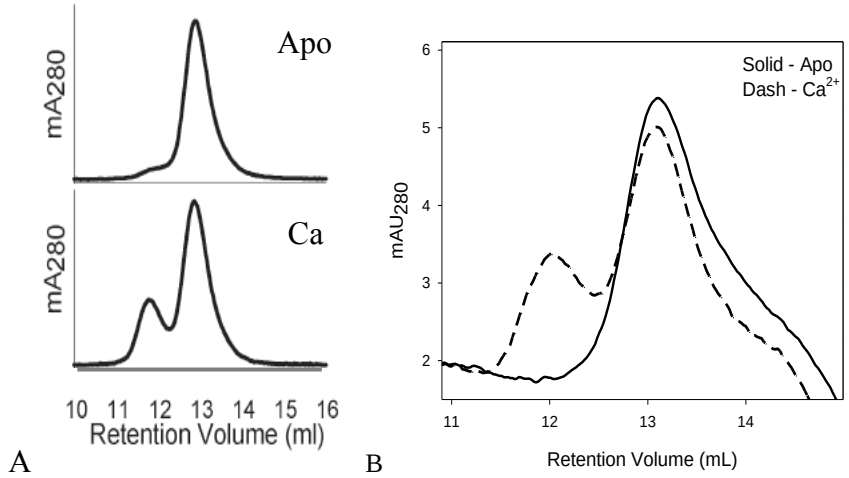

Figure 26. **Analytical SEC to determine dimer formation of as a function of calcium concentration**. The wild type (A) and NCAD 12_Q87C (B) were predominantly monomeric in the apo state (solid line) and a 70/30 mixture of monomer and dimer in the presence of 1 mM calcium (broken line).

To assess the effect of the mutation on dimerization, analytical size exclusion chromatography (SEC) was performed on wild type and NCAD 12_Q87C in the absence and presence of calcium (1 mM) with apo-mobile phase. In the apo state, both the wild type and NCAD12_Q87C showed that the protein was in the monomeric state (13.2 mL, ~ 90%; **Figure 26**). Upon addition of 1 mM calcium, SEC data showed two peaks (11.8 mL ± 0.1 mL and 13.2 mL ± 0.1 mL) indicating the presence of monomer (~70%) and dimer (~30%). Since WT and N-Q87C exhibited almost equal levels of the dimer, we conclude that the two proteins have similar dimerization affinity.

In summary, the effect of the Q87C mutation on the folding, stability and assembly properties was minimal. There was a small effect on the fluorescence signal change upon addition of calcium. This indicates a change in the calcium dependent change in the environment of one or both of the two tryptophan residues. Overall the stability and dimerization properties were unaffected. The bottom line is that we are confident that results from the following FRET

studies reflect properties of the wild type protein and are not significantly affected by the introduction of the mutation.

II.. Determination of labeling efficiencies of protein with donor and the acceptor fluorophore.

II.A. The labeling efficiency of AEDANS-Q87C

The labeling efficiency of the AEDANS derivatized protein NCAD 12-Q87C was determined by using UV-vis spectroscopy (**Figure 27**). The labeling efficiency for AEDANS-labeled protein was calculated by using equations 3.4 and 3.5. For AEDANS-labeled protein, the UV spectrum showed two absorption bands at 280 nm and 336 nm. According to the manufacturer's protocol (Invitrogen), the dye contributed 23% of absorption at 336 nm to the absorption at 280 nm. Based on the experimental data and calculations, AEDANS-Q87C protein concentration was 190 μM and dye concentration was 180 μM achieving 95% labeling efficiency.

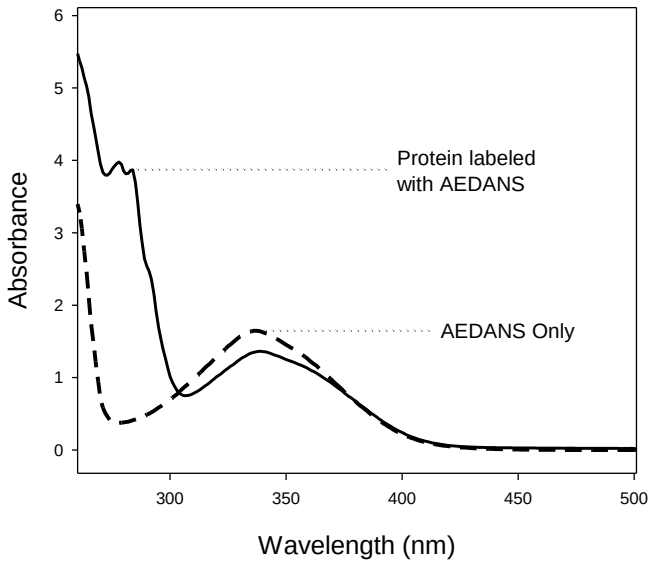

Figure 27. **UV spectra of AEDANS labeled NCAD 12_Q87C and AEDANS dye solution only**. Labeled NCAD 12_Q87C (solid line) displays the tryptophan absorption of the protein at 280 nm and AEDANS absorption at 336 nm. The IAEDANS dye only (dashed) exhibits the absorption at 336 nm.

II.B. Labeling efficiency of AF-Q87C

The labeling efficiency of the AF 488 derivatized protein NCAD 12-Q87C was determined by using UV-vis spectroscopy (**Figure 28**). The labeling efficiency for AF 488-labeled protein was calculated by using equations 3.7 and 3.8. For AF 488-labeled protein, the UV spectrum showed two absorption bands at 280 nm and 494 nm. According to the manufacturer's protocol (Invitrogen), the dye contributed 11% of absorption at 494 nm to the absorption at 280 nm. Based on the experimental data and calculations, AF-Q87C protein concentration was 120 μM and dye concentration was 70 μM achieving 60% labeling efficiency.

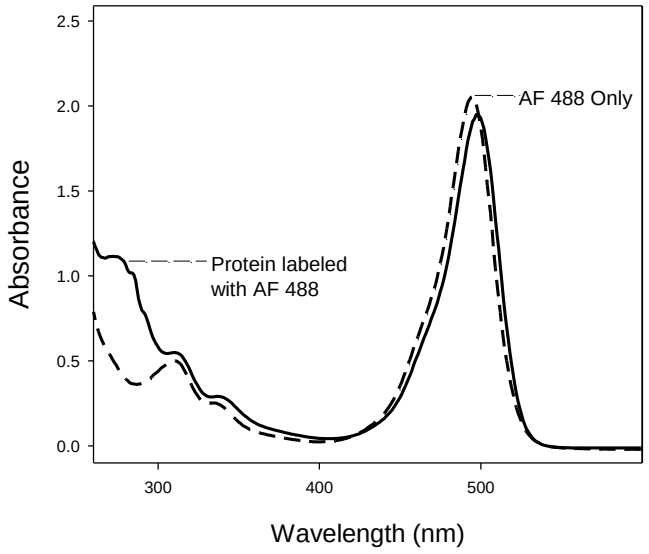

Figure 28. **UV spectra of AF-labeled NCAD 12-Q87C and free AF dye in SEC buffer**. Labeled NCAD 12_Q87C (solid line) displays the tryptophan absorption of the protein at 280 nm and AF absorption at 494 nm. The AF dye only (dashed) exhibits the absorption at 494 nm.

III. Fluorescence spectra of donor and acceptor proteins

III.A. Basic fluorescence spectra

The absorption and emission spectra from AEDANS and AF488 (**Figure 29**) are shown to illustrate that this pair is well-suited for energy transfer from donor to acceptor. There is complete overlap between the emission spectrum of donor and the excitation spectrum of acceptor. It also illustrates that there is significant overlap between the emission of donor and the

emission of acceptor. This creates a background signal of donor emission in the acceptor channel (bleed through) leading to an overestimation of FRET signal if not properly taken into account. The spectra on the right have been re-plotted to illustrate the actual magnitude of donor signals compared to an equimolar solution of acceptor. Thus, considering the magnitude of the spectral signals of the donor relative to the acceptor, the bleed through problem is not as profound as it appears in panel A. However, it is necessary to correct for bleed through (F_D) in the calculation of the FRET data. One can also see that there is a small, but significant absorption of energy at 370 nm for the acceptor. This leads to an additional contribution to the total fluorescence due to direct excitation of the acceptor. This value (F_A) will also be considered in the final calculations

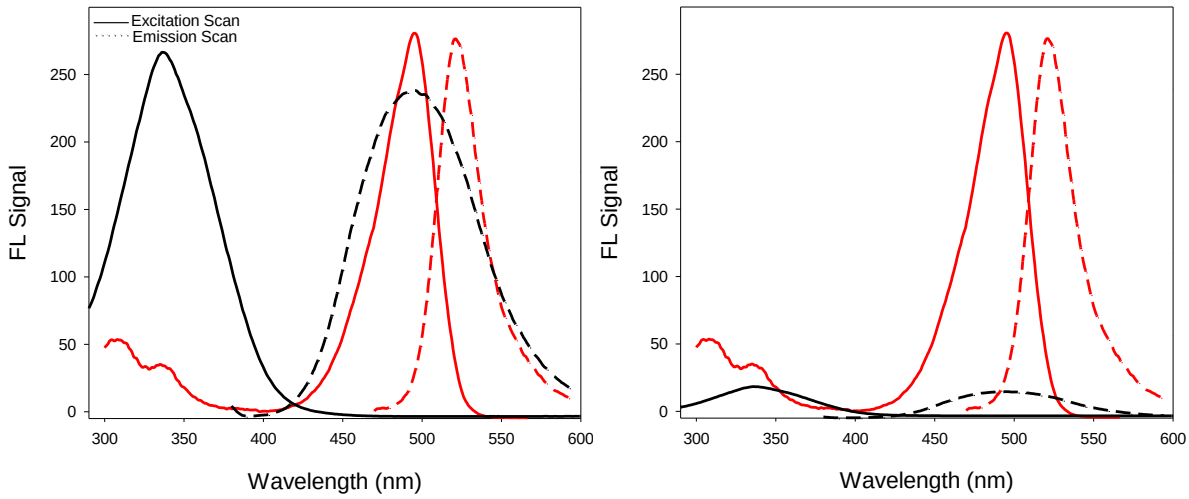

***Figure 29*. Fluorescence spectra of AEDANS-Q87C (donor) and AF-Q87C (acceptor).** The excitation (solid) and emission (dashed) spectra of AEDANS-Q87C (black) and AF-Q87C (red) are shown in each figure. The spectra on the left are shown ~ equal intensities of each spectrum. The figure on the right shows the relative signals of donor and acceptor.

IV. Demonstration of occurrence of FRET

IV.A. Spectra of pure donor and acceptor-labeled protein

Fluorescence spectra were conducted to determine whether or not FRET would occur after mixing donor and acceptor. **Figure 30** shows the proof of concept data; we observe FRET

between donor and acceptor fluorophores indicating the formation of dimer. Each spectral component will be discussed individually.

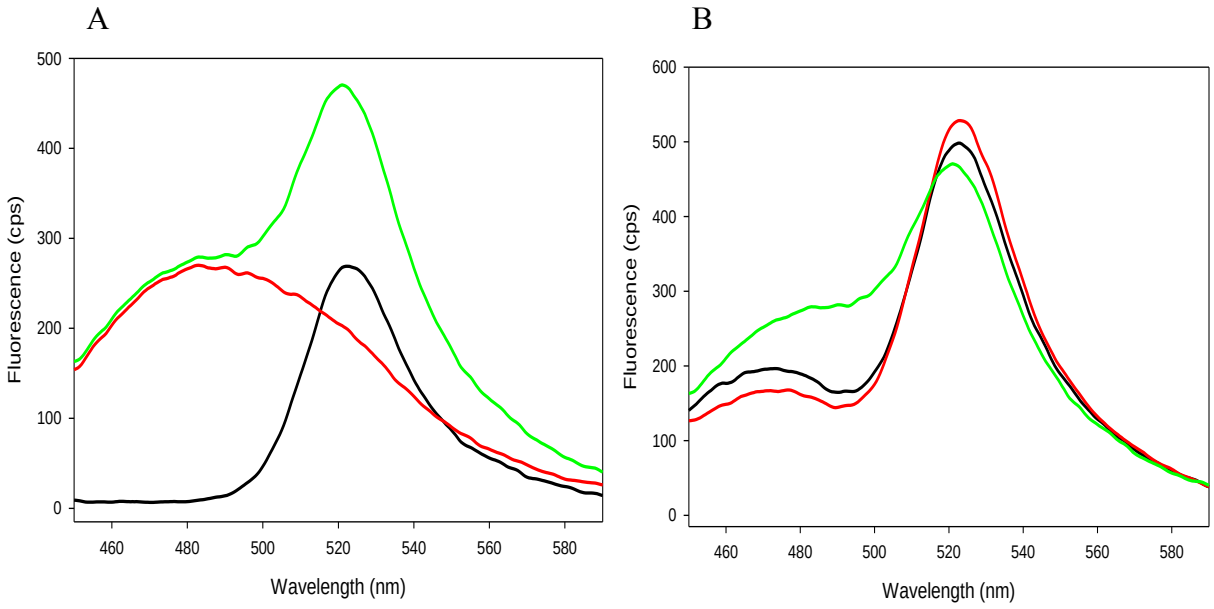

***Figure 30*. Determination of the occurrence of FRET**. (A) Excitation was 370 nm. Spectral signals from bleed through (F_D; red) and direct excitation of acceptor (AF-Q87C; F_A, black). The sum of F_A and F_D is the total background signal (green). (B) Again, excitation was 370 nm. The background signal form panel A is repotted (green). The total fluorescence (FT) is shown in the apo state (black) and with 1 mM calcium added (red). The difference between the green and red spectra represents the total FRET signal in the presence of calcium.

First we will discuss emission spectra individually which were measured before mixing donor and acceptor: the emission of acceptor, the emission of donor, and the sum of emissions from donor and acceptor. The black line in **Figure 30A** represents acceptor emission (F_A) with direct acceptor excitation. The acceptor was excited at wavelength 450 nm and had a maximum emission at 525 nm. The red line represents the donor emission (F_D) with direct donor excitation before titration. The donor was excited at wavelength 370 nm and exhibited the maximum emission at 490 nm followed by a long tailing emission that contributes a significant signal at 525 nm (the acceptor channel). The green line represents the sum of the individual signals from the donor and acceptor fluorophores at 525 nm (F_D+F_A). **Table 6** contains all of the relevant

wavelengths and signals for calculation of the background signals from direct excitation of acceptor and the bleed through signals from the donor.

***Table 6*: Spectral signals from pure donor and acceptor fluorophores**

Components	Conc. (μM)	Ex. λ_{max} (nm)	Em. λ_{max} (nm)	FL signal @ 525 nm
Acceptor (F_A)	20	450	525	266
Donor (F_D)	20	370	490	187
Sum ($F_A + F_D$)				453

VI.B. FRET occurs between donor- and acceptor-labeled proteins

After mixing donor and acceptor, the total fluorescence of the mixtures was measured using an excitation wavelength of 370 nm. This wavelength gives maximum excitation of the donor fluorophore and minimal excitation of the donor fluorophore. Emission spectra were taken in the absence and presence of calcium (1mM) (**Figure 30B**). Both the apo and calcium added spectra were greater than the sum of the background signals ($F_A + F_D$). This indicates that there is energy transfer between the donor and acceptor-labeled proteins; dimer is forming. Considering their emission intensity at 525 nm, the signal increase with the addition of 1 mM calcium confirmed the increased in the level of strand-crossover dimer in the presence of calcium The numerical values of the signals is shown in **Table 7**. This result proved that FRET did occur between AEDANS-Q87C and AF-Q87C. The FRET intensity in the presence of calcium is 38 cps (491-453).

***Table 7:* Differences in total fluorescence as a function of calcium**

Components	FL signal (at 525 nm)
Mixture $_{(A+D)apo}$ ($F_{T(apo)}$)	491
Mixture $_{(A+D)Ca^{2+}}$ ($F_{T(Ca\ 2+)}$)	524
Sum of $F_A + F_D$ ($F_{(A+D)}$)	453

It is important to note that after every addition of protein, not only was the total fluorescence measured, but also the contribution of the bleed through signal from donor emission (F_D) and the signal from direct excitation of acceptor (F_A) had to be determined. Because FRET signal was measured in mixed solutions of donor and acceptor labeled proteins, we did not have the advantage of being able to determine the F_A and F_D contributions as illustrated simply in **Figure 30A**. Thus, we had to do some preparatory work in order to get all 3 signals (F_T, F_D and F_A) from mixed solutions of acceptor- and donor-labeled proteins.

IV.C. Determining F_A in mixed solutions

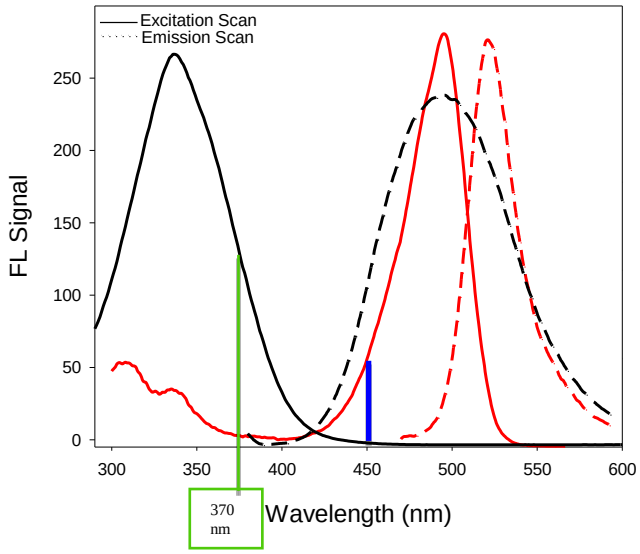

Figure 31. **Spectra of donor and acceptor**. Black lines represent spectra of donor: excitation (solid line) and emission (dashed line). Red lines represent spectra of acceptor: excitation (solid line) emission (dashed line). Green vertical line indicates the energy transfer wavelength 370 nm. Blue line indicates the direct excitation wavelength of acceptor.

To determine the level of F_A in mixed solutions of donor and acceptor-labeled proteins, we performed a simple experiment. Pure acceptor labeled protein was excited at 370 and 450 nm (**Figure 30 (A) and 31**). The emission spectrum resulting from excitation at 370 nm provides the intensity of the emission at 525 nm from direct excitation acceptor at the donor excitation wavelength (F_A). We also excited the pure acceptor solution at 450 nm and measured the

emission intensity at 525 nm. The ratio of these two emission intensities provides us with a correction factor that we can use to determine F_A. This was discussed previously in the experimental procedures chapter and summarized in Eq 3.9. The correction factor was 6.025; the signal of acceptor from direct excitation at donor excitation wavelengths was only $1/6^{th}$ of the intensity when exciting the acceptor at its maximum excitation wavelength of 450 nm.

In order to determine the effect of direct excitation of the acceptor in mixed solutions of donor and acceptor-labeled protein, we had the advantage of being able to excite acceptor exclusively at 450 nm, a wavelength that will not excite donor fluorophore. So, by exciting the acceptor at 450 nm, we can get the total fluorescence emission for the acceptor. Using the correction factor, we calculated F_A signal.

IV.D. Determination of the bleed through signal

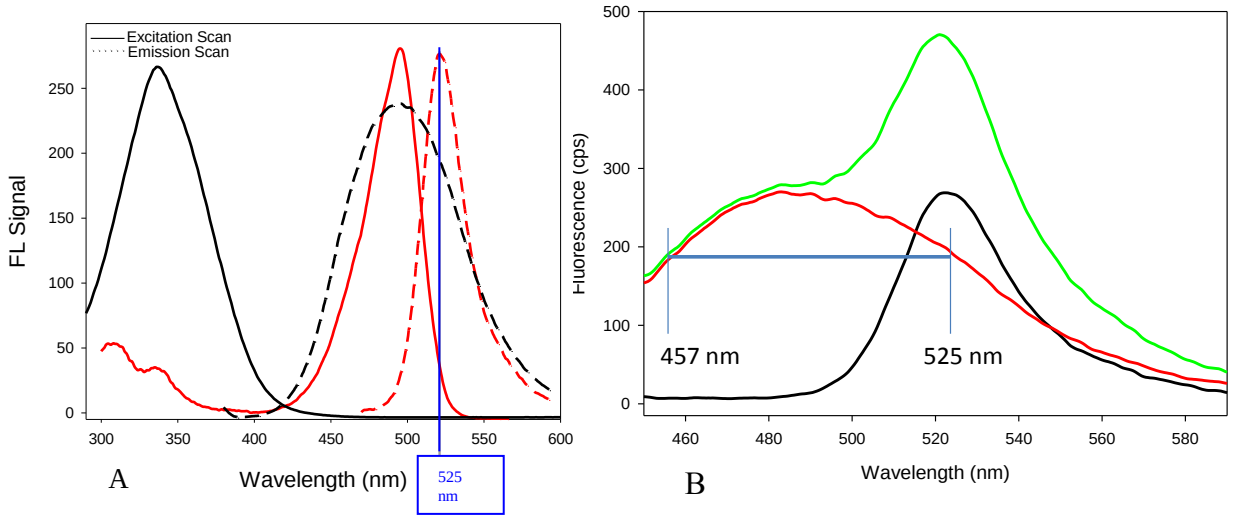

Figure 32. **Determination of the bleed through signal**. Figure A and B show that the emission of donor overlaps with FRET channel at 525 nm. The emission signal at 525 nm of donor-labeled protein cannot be determined in mixed solutions containing acceptor-labeled protein. But we know that the signals of donor at 525 nm and 457 nm are identical (B panel). So, we can use the signal at 457 nm to indicate the contribution of bleed through to the signal at 525 nm.

Next, we had to account for the donor emission that overlaps with the FRET channel and artificially inflates the apparent FRET signal. Because donor signal cannot be measured

independently once acceptor has been added, we have to estimate the contribution of the donor (F_D) to the total fluorescence signal (F_T). In the interval 450 ~ 470 nm, donor signal dominated the emission spectrum (see **Figure 32 (A) and (B)**). In pure solutions of donor-labeled protein, we found that the signal at 457 nm (188.6 (cps)) was numerically identical to the signal of donor at 525 nm (189.3 (cps)). In mixed solutions, there was no contribution of acceptor emission to the total fluorescence signal. So, we can use the fluorescence emission at 457 nm to indicate the contribution of donor signal to the total fluorescence in mixed solutions of donor- and acceptor-labeled proteins.

V. Determination of K_d using FRET

In this experiment, we titrate a dilute solution of acceptor-labeled protein against a concentrated solution of donor-labeled protein. The actual raw data is shown in **Figure 33** below. There were two types of titrations performed. Data from each will be discussed individually. First, a 5 μM solution of acceptor-labeled protein was placed in the cuvette and titrated with a concentrated solution of donor-labeled protein (closed symbols). One can see that the F_A signal decreased as the acceptor was diluted from each successive addition of donor-labeled protein. As one would expect, the donor signal increased with each addition because it is being added. Note that the total fluorescence signal (F_T) also increased and is necessarily greater than F_D. The majority of F_T is from the F_D.

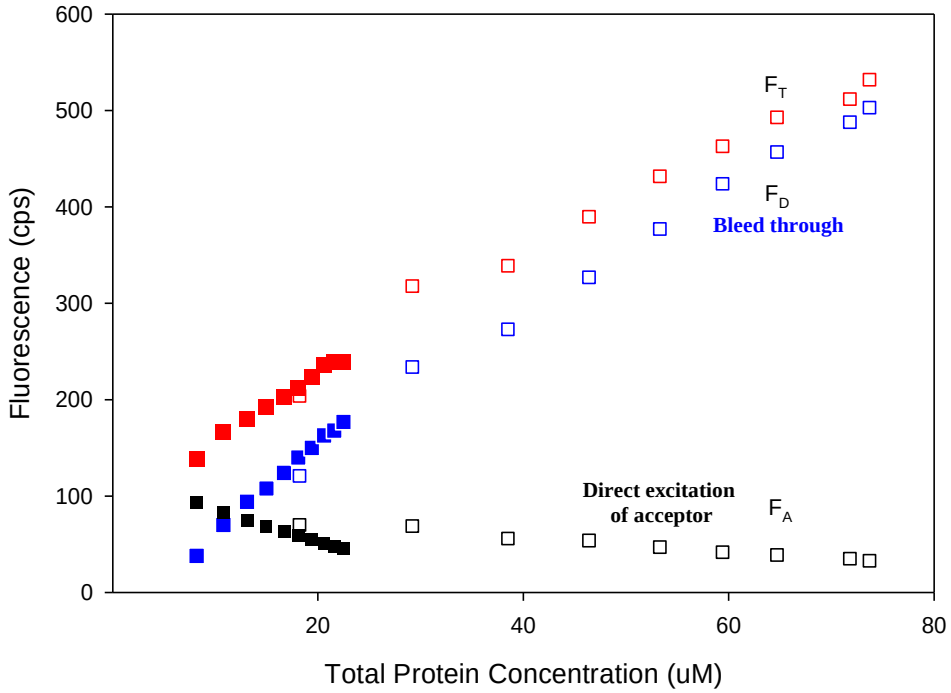

***Figure 33*. Fluorescence signal as a function of total protein concentration.** The fluorescence emission signals for the total fluorescence (F_T; red), the bleed through of donor signal in the acceptor channel (F_D; blue) and the direct excitation of acceptor at the donor excitation wavelength (F_A; black). In each case, the excitation wavelength is 370 nm and emission wavelength is 525 nm. Forward (closed) and reverse (open) titration data are shown.

The second titration was a reverse titration where concentrated donor-labeled protein was in the cuvette and a dilute solution of acceptor-labeled protein was added to it (open symbols). Here the donor signal decreased and the acceptor signal increased. From these data the total FRET signal can be calculated from a simple equation.

$$FRET = F_T - F_A - F_D \qquad (4.1)$$

Thus, at every point in the titration, a value for FRET, D_t (concentration of donor) and C_t (total protein concentration) can be calculated. In the figure below, $FRET/F_A$ is plotted versus the C_t.

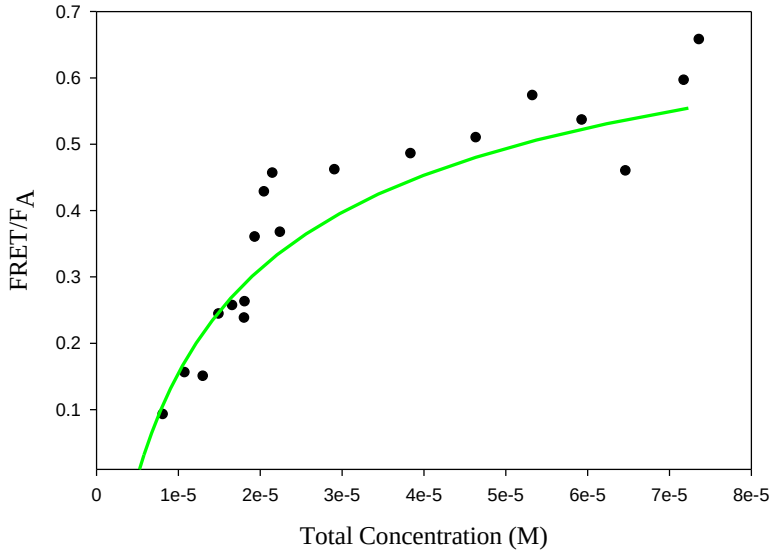

***Figure 34*. Experimental data of FRET as a function of total concentration**. FRET value was calculated from Eq 4.1. Total concentration is the sum of the D_t and A_t concentrations.

The data is **Figure 34** was fit to Eq 2.9 to resolve values for F_C, the limiting value for the ratio $FRET/F_A$, and K_d, the equilibrium dimer dissociation constant. Results are reported in **Table 8** and literature values of K_d are shown in **Table 8** below:

***Table 8:* Parameters resolved from analysis of the FRET experiment**

Fit #	K_d (M^{-1})	F_C
1	$43 \pm 2 \times 10^{-6}$	1.1 ± 0.1
2	$25 \pm 3 \times 10^{-6}$	<0.9>

***Table 9*. K_ds for the homodimerization of NCAD 12 constructs.**

Species[a]	N-cadherin EC1-2 (μM)	Method
Mouse	25. 8 ± 1.5 [26]	Equilibrium analytical ultracentrifugation (AUC)
Mouse	28. 1 ± 4.0 [37]	Size exclusion chromatograph
Human	24. 6 ± 5.0 [26]	Equilibrium analytical ultracentrifugation (AUC)

[a] Experiments performed at 25°C on two domain constructs

VI. Conclusions

Our research focuses on domains one and two of the extracellular region, a minimal subunit for cadherin function. Recent studies from our lab showed a dramatic calcium-dependent difference in the kinetics of neural (N-) and epithelial (E-) cadherins dimer disassembly, which may have a physiologically relevant role. This motivated our interest to study whether there is a geometrical factor for these kinetically different dimeric states. To investigate these geometrical factors we need to develop and perform a series of bulk and single molecule methods that use Förster Resonance Energy Transfer (FRET) phenomenon.

We established that the mutation Q87C did not change the structure, stability, and function of the protein. We observed the FRET phenomenon when we mixed the acceptor and donor. These results imply that the 87^{th} in the amino acid sequence was a good choice to monitor the dimerization of N-cadherin. We were able to demonstrate that the FRET signal varies in a predictable way with the concentration of protein. The data fit well to the predicted relationship shown in Eq 2.9. Although the resolved value for K_d depends upon the values for F_C, when both parameters were allowed to vary, we resolved a value for the K_d that is less than a factor of 2 greater than the expected value based on other studies (37). If we fix the value of F_C to 0.9, we resolve the value for K_d exactly. Our resolved K_d (25.0 ± 3.0 μM) was in agreement with literature values (K_d = 25. 8 ± 1.5 μM; K_d = 28. 1 ± 4.0 μM). These studies will provide a new method to characterize the kinetics of dimerization of epithelial and neural cadherins and to determine orientation of kinetically distinct protomers in single molecule studies in the future.

BIBLIOGRAPHY

1. Takeichi, M., Morphogenetic roles of classic cadherins, *Curr Opin Cell Biol, 7*, 619 (1995).
2. Gumbiner, B. M., Cell adhesion: the molecular basis of tissue architecture and morphogenesis, *Cell, 84*, 345 (1996).
3. Tepass, U., Truong, K., Godt, D., Ikura, M., and Peifer, M., Cadherins in embryonic and neural morphogenesis, *Nat Rev Mol Cell Biol, 1*, 91 (2000).
4. Shapiro, L., and Weis, W. I., Structure and biochemistry of cadherins and catenins, *Cold Spring Harb Perspect Biol, 1*, a003053 (2009).
5. Watanabe, T., Sato, K., and Kaibuchi, K., Cadherin-mediated intercellular adhesion and signaling cascades involving small GTPases, *Cold Spring Harb Perspect Biol, 1*, a003020 (2009).
6. Redies, C., Cadherins in the central nervous system, *Prog Neurobiol, 61*, 611 (2000).
7. Shapiro, L., Love, J., and Colman, D. R., Adhesion molecules in the nervous system: structural insights into function and diversity, *Annu Rev Neurosci, 30*, 451 (2007).
8. Yu, X., and Malenka, R. C., Multiple functions for the cadherin/catenin complex during neuronal development, *Neuropharmacology, 47*, 779 (2004).
9. Huntley, G. W., Gil, O., and Bozdagi, O., The cadherin family of cell adhesion molecules: multiple roles in synaptic plasticity, *Neuroscientist, 8*, 221 (2002).
10. Christofori, G., and Semb, H., The role of the cell-adhesion molecule E-cadherin as a tumour-suppressor gene, *Trends Biochem Sci, 24*, 73 (1999).
11. Stemmler, M. P., Cadherins in development and cancer, *Mol Biosyst, 4*, 835 (2008).
12. Chothia, C., and Jones, E. Y., The molecular structure of cell adhesion molecules, *Annu Rev Biochem, 66*, 823 (1997).

13. Troyanovsky, R. B., Laur, O., and Troyanovsky, S. M., Stable and unstable cadherin dimers: mechanisms of formation and roles in cell adhesion, *Mol Biol Cell, 18*, 4343 (2007).

14. Ozawa, M., Lateral dimerization of the E-cadherin extracellular domain is necessary but not sufficient for adhesive activity, *J Biol Chem, 277*, 19600 (2002).

15. Fujiyama, F., Stephenson, F. A., and Bolam, J. P., Synaptic localization of GABA(A) receptor subunits in the substantia nigra of the rat: effects of quinolinic acid lesions of the striatum, *Eur J Neurosci, 15*, 1961 (2002).

16. Knott, G. W., Quairiaux, C., Genoud, C., and Welker, E., Formation of dendritic spines with GABAergic synapses induced by whisker stimulation in adult mice, *Neuron, 34*, 265 (2002).

17. Okada, D., Ozawa, F., and Inokuchi, K., Input-specific spine entry of soma-derived Vesl-1S protein conforms to synaptic tagging, *Science, 324*, 904 (2009).

18. Mendez, P., De Roo, M., Poglia, L., Klauser, P., and Muller, D., N-cadherin mediates plasticity-induced long-term spine stabilization, *J Cell Biol, 189*, 589 (2010).

19. Pearson, W., *LALIGN - find multiple matching subsegments in two sequences* (2009).

20. Tamura, K., Shan, W. S., Hendrickson, W. A., Colman, D. R., and Shapiro, L., Structure-function analysis of cell adhesion by neural (N-) cadherin, *Neuron, 20*, 1153 (1998).

21. Harrison, O. J., Jin, X., Hong, S., Bahna, F., Ahlsen, G., Brasch, J., Wu, Y., Vendome, J., Felsovalyi, K., Hampton, C. M., Troyanovsky, R. B., Ben-Shaul, A., Frank, J., Troyanovsky, S. M., Shapiro, L., and Honig, B., The extracellular architecture of adherens junctions revealed by crystal structures of type I cadherins, *Structure, 19*, 244 (2011).

22. Shapiro, L., Fannon, A. M., Kwong, P. D., Thompson, A., Lehmann, M. S., Grubel, G., Legrand, J. F., Als-Nielsen, J., Colman, D. R., and Hendrickson, W. A., Structural basis of cell-cell adhesion by cadherins [see comments], *Nature, 374*, 327 (1995).

23. Boggon, T. J., Murray, J., Chappuis-Flament, S., Wong, E., Gumbiner, B. M., and Shapiro, L., C-cadherin ectodomain structure and implications for cell adhesion mechanisms, *Science, 296*, 1308 (2002).

24. Parisini, E., Higgins, J. M., Liu, J. H., Brenner, M. B., and Wang, J. H., The crystal structure of human E-cadherin domains 1 and 2, and comparison with other cadherins in the context of adhesion mechanism, *J Mol Biol, 373*, 401 (2007).

25. Shapiro, L., Kwong, P. D., Fannon, A. M., Colman, D. R., and Hendrickson, W. A., Considerations on the folding topology and evolutionary origin of cadherin domains, *Proc Natl Acad Sci U S A, 92*, 6793 (1995).

26. Katsamba, P., Carroll, K., Ahlsen, G., Bahna, F., Vendome, J., Posy, S., Rajebhosale, M., Price, S., Jessell, T. M., Ben-Shaul, A., Shapiro, L., and Honig, B. H., Linking molecular affinity and cellular specificity in cadherin-mediated adhesion, *Proc Natl Acad Sci U S A, 106*, 11594 (2009).

27. Haussinger, D., Ahrens, T., Aberle, T., Engel, J., Stetefeld, J., and Grzesiek, S., Proteolytic E-cadherin activation followed by solution NMR and X-ray crystallography, *Embo J, 23*, 1699 (2004).

28. Patel, S. D., Ciatto, C., Chen, C. P., Bahna, F., Rajebhosale, M., Arkus, N., Schieren, I., Jessell, T. M., Honig, B., Price, S. R., and Shapiro, L., Type II cadherin ectodomain structures: implications for classical cadherin specificity, *Cell, 124*, 1255 (2006).

29. Pertz, O., Bozic, D., Koch, A. W., Fauser, C., Brancaccio, A., and Engel, J., A new crystal structure, Ca2+ dependence and mutational analysis reveal molecular details of E-cadherin homoassociation, *Embo J, 18*, 1738 (1999).

30. Haussinger, D., Ahrens, T., Sass, H. J., Pertz, O., Engel, J., and Grzesiek, S., Calcium-dependent homoassociation of E-cadherin by NMR spectroscopy: changes in mobility, conformation and mapping of contact regions, *J Mol Biol, 324*, 823 (2002).

31. Overduin, M., Harvey, T. S., Bagby, S., Tong, K. I., Yau, P., Takeichi, M., and Ikura, M., Solution structure of the epithelial cadherin domain responsible for selective cell adhesion, *Science, 267*, 386 (1995).

32. Overduin, M., Tong, K. I., Kay, C. M., and Ikura, M., 1H, 15N and 13C resonance assignments and monomeric structure of the amino-terminal extracellular domain of epithelial cadherin, *J Biomol NMR, 7*, 173 (1996).

33. Miloushev, V. Z., Bahna, F., Ciatto, C., Ahlsen, G., Honig, B., Shapiro, L., and Palmer, A. G., 3rd, Dynamic properties of a type II cadherin adhesive domain: implications for the mechanism of strand-swapping of classical cadherins, *Structure, 16*, 1195 (2008).

34. He, W., Cowin, P., and Stokes, D. L., Untangling desmosomal knots with electron tomography, *Science, 302*, 109 (2003).

35. Shan, W. S., Tanaka, H., Phillips, G. R., Arndt, K., Yoshida, M., Colman, D. R., and Shapiro, L., Functional cis-heterodimers of N- and R-cadherins, *J Cell Biol, 148*, 579 (2000).

36. Harrison, O. J., Corps, E. M., Berge, T., and Kilshaw, P. J., The mechanism of cell adhesion by classical cadherins: the role of domain 1, *J Cell Sci, 118*, 711 (2005).

37. Vunnam, N., Flint, J., Balbo, A., Schuck, P., and Pedigo, S., Dimeric States of Neural- and Epithelial-Cadherins are Distinguished by the Rate of Disassembly, *Biochemistry, 50*, 2951 (2011).

38. Vunnam, N., and Pedigo, S., Calcium-induced strain in the monomer promotes dimerization in neural cadherin, *Biochemistry, 50*, 8437 (2011).

39. Harrison, O. J., Corps, E. M., and Kilshaw, P. J., Cadherin adhesion depends on a salt bridge at the N-terminus, *J Cell Sci, 118*, 4123 (2005).

40. Vunnam, N., and Pedigo, S., Sequential binding of calcium leads to dimerization in neural cadherin, *Biochemistry, 50,* 2973 (2011).

41. Courjean, O., Chevreux, G., Perret, E., Morel, A., Sanglier, S., Potier, N., Engel, J., van Dorsselaer, A., and Feracci, H., Modulation of E-cadherin monomer folding by cooperative binding of calcium ions, *Biochemistry, 47*, 2339 (2008).

42. Ozawa, M., Engel, J., and Kemler, R., Single amino acid substitutions in one Ca2+ binding site of uvomorulin abolish the adhesive function, *Cell, 63*, 1033 (1990).

43. Prakasam, A., Chien, Y. H., Maruthamuthu, V., and Leckband, D. E., Calcium site mutations in cadherin: impact on adhesion and evidence of cooperativity, *Biochemistry, 45*, 6930 (2006).

44. Baumgartner, W., Golenhofen, N., Grundhofer, N., Wiegand, J., and Drenckhahn, D., Ca2+ dependency of N-cadherin function probed by laser tweezer and atomic force microscopy, *J Neurosci, 23*, 11008 (2003).

45. Perret, E., Benoliel, A. M., Nassoy, P., Pierres, A., Delmas, V., Thiery, J. P., Bongrand, P., and Feracci, H., Fast dissociation kinetics between individual E-cadherin fragments revealed by flow chamber analysis, *Embo J, 21*, 2537 (2002).

46. Perret, E., Leung, A., Feracci, H., and Evans, E., Trans-bonded pairs of E-cadherin exhibit a remarkable hierarchy of mechanical strengths, *Proc Natl Acad Sci U S A, 101*, 16472 (2004).

47. Mysore, S. P., Tai, C. Y., and Schuman, E. M., N-cadherin, spine dynamics, and synaptic function, *Front Neurosci, 2*, 168 (2008).

48. Harrison, O. J., Bahna, F., Katsamba, P. S., Jin, X., Brasch, J., Vendome, J., Ahlsen, G., Carroll, K. J., Price, S. R., Honig, B., and Shapiro, L., Two-step adhesive binding by classical cadherins, *Nat Struct Mol Biol, 17*, 348 (2010).

49. Vunnam, N., and Pedigo, S., X-interface is not the explanation for the slow disassembly of N-cadherin dimers in the apo state, *Protein Sci, 21*, 1006 (2012).

50. Bekirov, I. H., Needleman, L. A., Zhang, W., and Benson, D. L., Identification and localization of multiple classic cadherins in developing rat limbic system, *Neuroscience, 115*, 213 (2002).

51. Brasch, J., Harrison, O. J., Honig, B., and Shapiro, L., Thinking outside the cell: how cadherins drive adhesion, *Trends Cell Biol, 22*, 299 (2012).

52. Sivasankar, S., Zhang, Y., Nelson, W. J., and Chu, S., Characterizing the initial encounter complex in cadherin adhesion, *Structure, 17*, 1075 (2009).

53. Hong, S., Troyanovsky, R. B., and Troyanovsky, S. M., Cadherin exits the junction by switching its adhesive bond, *J Cell Biol, 192*, 1073 (2011).

54. Lakowicz, J. R., *Principles of Fluorescene Spectroscopy*, Kluwer Academic/Plenum Publishers, New York (1999).

55. Song, Y., Madahar, V., and Liao, J., Development of FRET assay into quantitative and high-throughput screening technology platforms for protein-protein interactions, *Ann Biomed Eng, 39*, 1224 (2011).

56. Roy, R., Hohng, S., and Ha, T., A practical guide to single-molecule FRET, *Nat Methods, 5*, 507 (2008).

57. Tinoco, I., Jr., and Gonzalez, R. L., Jr., Biological mechanisms, one molecule at a time, *Genes Dev, 25*, 1205 (2011).

58. Loura, L. M., Simple Estimation of Forster Resonance Energy Transfer (FRET) Orientation Factor Distribution in Membranes, *Int J Mol Sci, 13*, 15252 (2012).

59. Eisinger, J., and Dale, R. E., What has energy transfer done for biochemistry lately? , in *Excited States of Biological Molecules*, Birks, J., Ed., pp. 579 590 (1974).

60. Dale, R. E., Eisinger, J., and Blumberg, W. E., The orientational freedom of molecular probes. The orientation factor in intramolecular energy transfer, *Biophys J, 26*, 161 (1979).

61. Jia, H., Satumba, W. J., Bidwell, G. L., 3rd, and Mossing, M. C., Slow assembly and disassembly of lambda Cro repressor dimers, *J Mol Biol, 350*, 919 (2005).

62. Fraczkiewicz, R., and Braun, W., Exact and efficient calculation of the accessible surface areas and their gradients for macromolecules, *J. Comp. Chem., 19*, 319 (1998).

63. Pace, C. N., Vajdos, F., Fee, L., Grimsley, G., and Gray, T., How to measure and predict the molar extinction coefficient of a protein, *Protein Sci, 4*, 2411 (1995).

64. Prasad, A., Housley, N. A., and Pedigo, S., Thermodynamic stability of domain 2 of epithelial cadherin, *Biochemistry, 43*, 8055 (2004).

65. Pokutta, S., Herrenknecht, K., Kemler, R., and Engel, J., Conformational changes of the recombinant extracellular domain of E- cadherin upon calcium binding, *Eur J Biochem, 223*, 1019 (1994).

66. Alattia, J. R., Ames, J. B., Porumb, T., Tong, K. I., Heng, Y. M., Ottensmeyer, P., Kay, C. M., and Ikura, M., Lateral self-assembly of E-cadherin directed by cooperative calcium binding, *FEBS Lett, 417*, 405 (1997).

67. Greenfield, N., and Fasman, G. D., Computed circular dichroism spectra for the evaluation of protein conformation, *Biochemistry, 8*, 4108 (1969).

68. Woody, R. W., Theory of Circular Dichroism, in *Circular Dichroism and the Conformational Analysis of Biomolecules*, Fasman, G. D., Ed., Plenum Press, New York, pp. 25 (1996).

VITA

XIAOYUN HOWARD

313 Tanner Dr. • Oxford, MS 38655 • (662)513-5914 • xzhoward@go.olemiss.edu

EDUCATION

M.S., Biochemistry, University of Mississippi, August 2013
Thesis: Determination of Dimer Dissociation Constant of Neural cadherin by Fluorescence Resonance Energy Transfer

B.A., Biochemistry, University of Mississippi, May 2007

RESEARCH EXPERIENCE

Research Assistant, 2011 – 2013
University of Mississippi

TEACHING EXPERIENCE

Teaching Assistant, 2009 – 2011
University of Mississippi,
Courses: General Chemistry Labs